Tropical cirrus evolution in a km-scale model with improved ice microphysics

Blaž Gasparini[1], Rachel Atlas[2], Aiko Voigt[1], Martina Krämer[3,4], and Peter N. Blossey[5]

[1]Department of Meteorology and Geophysics, University of Vienna, Vienna, Austria
[2]CNRS-Laboratoire de Météorologie Dynamique, LMD, Palaiseau, France
[3]Institute for Atmospheric Physics, University of Mainz, Mainz, Germany
[4]IEK-7, Forschungszentrum Jülich, Jülich, Germany
[5]Department of Atmospheric and Climate Science, University of Washington, Seattle, USA

Correspondence: Blaž Gasparini (blaz.gasparini@univie.ac.at)

Abstract.

Tropical cirrus clouds form ~~via~~ through in situ ice nucleation below the homogeneous freezing temperature of water or through detrainment from deep convection. Despite their importance, limited understanding of their evolution and formation pathways contributes to large uncertainty in climate projections. To address these challenges, we implement novel passive tracers in the System for Atmospheric Modeling (SAM) cloud-resolving model ~~SAM~~ to track the three-dimensional development of cirrus clouds. One tracer tracks air parcels exiting convective updrafts, revealing a rapid decline in ice crystal size and number as anvils age. Another tracer focuses on in situ cirrus, capturing their formation in the cold upper atmosphere and the subsequent reduction in their ice crystal number over time. We find that in situ cirrus dominate at colder temperatures and lower ice water contents, while anvil cirrus prevail at temperatures ~~above~~ ≥ -60°C. ~~Although~~ Despite the frequent occurrence of in situ cirrus ~~have a smaller radiative impact compared to anvil cirrus, their contribution must be considered when evaluating~~ within the tropical tropopause layer, they account for only 6-7% of the total tropical cirrus cloud top-of-the-atmosphere radiative ~~effects~~effect. These findings improve our ability to assess the distinct roles of convective and in situ cirrus in shaping tropical cirrus properties and their impacts on climate.

We also improve the model's representation of tropical cirrus through simple, computationally inexpensive microphysics modifications, ~~achieving better~~ improving agreement with tropical aircraft observations. We show that updrafts critical for tropical cirrus formation are only resolved ~~at horizontal grid spacings finer than~~ in our simulations at a horizontal grid spacing of 250 m ~~—~~ – much finer than those used in global storm-resolving models. ~~To mitigate this limitation, we propose microphysics improvements that reduce biases without increasing computational costs.~~

1 Introduction

Tropical cirrus clouds, defined as ice clouds with tops at temperatures colder than -40°C, dominate regions of tropical ascent in both cloud fraction and radiative effects (Berry and Mace, 2014; Hartmann and Berry, 2017). These clouds are diverse, with their origins and properties shaped by distinct formation mechanisms: convective cirrus originating from deep convective updrafts and in situ cirrus that are formed by ice nucleation in the cold tropical upper troposphere. Understanding the relative contributions and characteristics of these two cloud types is crucial for improving their representation in atmospheric models. The distinction between convective and in situ cirrus has practical implications for climate projections, as their formation mechanisms may respond differently to greenhouse gas forcing, potentially leading to different cloud feedbacks.

Convective cirrus, or anvil clouds, are initially thick and optically dense but rapidly lose mass through precipitation as they spread horizontally over large areas ~~(Deng et al., 2016)~~(Gasparini et al., 2021). Over time, they evolve into thinner clouds, often with optical depths of 1 to 2, which represent the most common form of tropical cirrus (Sokol and Hartmann, 2020). In contrast, in situ cirrus typically form in the tropical tropopause layer (TTL), above the mean detrainment level of convection. These clouds arise from ice nucleation triggered by small-scale dynamical processes, such as gravity wave-induced ~~fluctuations (Hoyle et al., 2005; Jensen et al., 2013)~~temperature and wind fluctuations (Hoyle et al., 2005; Kim et al., 2016; Chang and Ecuyer, 2020; E
. Unlike anvils, in situ cirrus are optically thin and display distinct microphysical properties, such as ~~very small ice crystals~~ ice crystals smaller than 20 μm (Krämer et al., 2020).

This study focuses on the lifecycle and microphysical evolution of both anvil and in situ cirrus. Snapshots or long-term averages of cloud properties, typically provided by model output or observations, do not reveal enough information to fully understand the processes that shape tropical cirrus. Lagrangian methods, such as tracking cloud properties using trajectories, have been widely used in both models (Wernli et al., 2016; Gasparini et al., 2021; Sullivan et al., 2022) and observations (Horner and Gryspeerdt, 2023; Jeggle et al., 2024). Passive tracers, an alternative approach to disentangle the origin and evolution of cirrus clouds, are more flexible in their use compared to trajectories, easier to implement, and computationally more efficient.

Tropical cirrus formation is shaped by processes spanning a wide range of spatial and temporal scales, from microphysical mechanisms such as ice nucleation, deposition, and sublimation, to dynamical influences including gravity waves, turbulence, and mesoscale circulations (Corcos et al., 2023; Jensen et al., 2024; Gasparini et al., 2022). However, even the most advanced models struggle to capture these complexities. Anvils originate in deep convective updrafts, which are unresolved in traditional general circulation models (GCMs). Although global storm-resolving models (GSRMs) with kilometer-scale grid spacings capture larger-scale convective dynamics, they fail to resolve the fine-scale dynamics critical to both anvil and in situ cirrus lifecycle (Atlas and Bretherton, 2023; Köhler et al., 2023; Achatz et al., 2024).

Moreover, GSRMs show large variability in simulating the microphysical properties of tropical cirrus (Atlas et al., 2024) and their radiative effects (Turbeville et al., 2022), sometimes performing worse than traditional GCMs. This reflects the trade-offs inherent in GSRMs, where the computational costs of high horizontal resolution are typically offset by simplified parameterizations of subgrid processes, particularly cloud microphysics.

In this work, we demonstrate that simple and inexpensive modifications to cloud microphysics can largely improve the simulation of tropical cirrus. By tracking cloudy air parcels from detrainment or in situ nucleation, we identify key differences in their lifecycle and microphysical properties, offering new insights into their respective contributions to tropical cirrus climatology and their radiative impacts. Furthermore, while kilometer-scale GSRMs can resolve updrafts near deep convection, we show that the dynamics critical for cirrus cloud formation in non-convective regions are only resolved at hectometer-scale grid spacings. These findings highlight some limitations of current modeling approaches and provide a pathway toward a more accurate representation of tropical cirrus in climate models.

2 Methods

2.1 Model

We use the System for Atmospheric Modeling (SAM) cloud resolving model (Khairoutdinov and Randall, 2003) version 6.10.9. SAM uses a 1.5-order Smagorinsky-type closure scheme to represent subgrid-scale turbulence and subgrid-scale motions. The timestep in SAM is adaptive and set based on the Courant-Friedrich-Levy criterion, that typically leads to a timestep of about 4.5 s for simulations at the horizontal grid spacing of 1 km. Radiative fluxes and heating rates are computed with ~~RRTMG (Mlawer et al., 1997; Iacono et al., 2008)~~the Rapid Radiative Transfer Model for GCMs (RRTMG, Mlawer et al., 1997; Iacono et al., 2008 , which is called every three minutes. Cloud and precipitation processes use the Predicted Particle Property (P3, Morrison and Milbrandt, 2015) microphysical scheme version 3.1.14.

2.1.1 Description and issues of ice nucleation in the standard P3 scheme

In mixed-phase conditions, ice crystals are formed by the following processes (Fig. 1 a):

- *Immersion freezing of cloud droplets and rain*: a volume-dependent formulation from Bigg (1953) with parameters following Barklie and Gokhale (1959).
- *Deposition nucleation*: a temperature-dependent formulation by Cooper (1986) that is limited to relative humidities with respect to ice (RH_{ice}) of $>$ 105% and temperatures colder than -15° C. Alternatively, a supersaturation-dependent Meyers et al. (1992) parameterization can be used. The maximum number of newly nucleated ice crystals ~~is~~ for both deposition freezing mechanisms is limited to 0.1 cm^{-3} s^{-1}.
- *Homogeneous freezing of cloud droplets and rain* which occurs instantaneously at a temperature of -40°C.

~~At temperatures colder than -40°C, ice~~ Ice crystals continue to be nucleated ~~by~~ at temperatures below -40°C using the Cooper (1986) or Meyers et al. (1992) ~~nucleation. In reality~~parameterizations, even though these schemes are not designed for such conditions. Moreover, nucleation events at such cold temperatures always lead to ice crystal concentrations of 0.1 cm^{-3} s^{-1}, as set by the ice nucleation limit. ~~Similar~~ Such approach therefore cannot lead to realistic cloud microphysical properties. Nevertheless, similar approaches to ice nucleation are used in a large number of microphysical schemes beyond the one used here (e.g. Morrison et al., 2005; Thompson et al., 2008).

2.1.2 Modifications to ice nucleation: mixed-phase freezing

~~Deposition nucleation parameterizations by Cooper (1986) and Meyers et al. (1992) are based on data from mixed-phase regime and thus should not be active at temperatures colder than the homogeneous freezing temperature of water. We thus~~ Due to issues

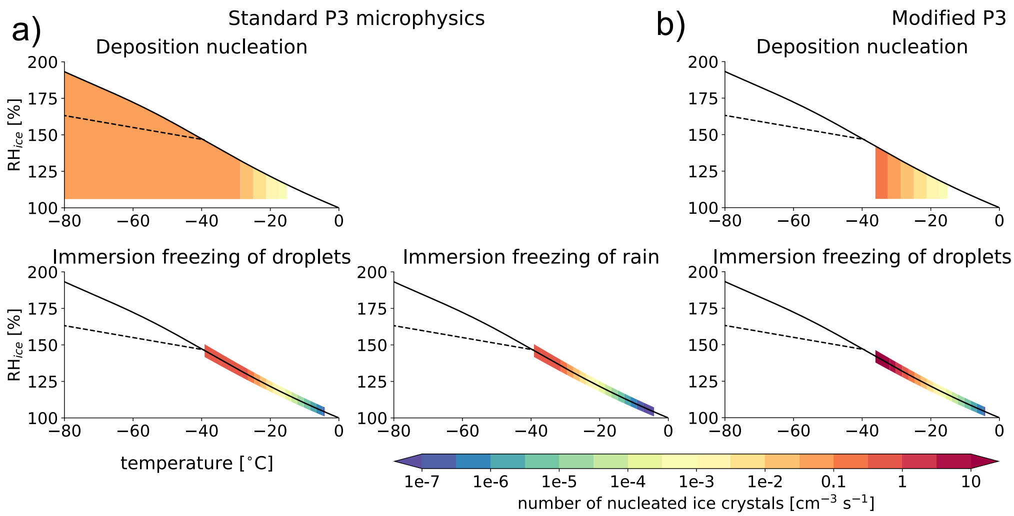

Figure 1. A visualization of the number of nucleated ice crystals from ice nucleating schemes in (a) the standard P3 freezing scheme and (b) its modified version. Solid line represents water saturation, dashed line represents the homogeneous nucleation limit following Koop et al. (2000).

with freezing parameterizations discussed above, we limit the deposition nucleation parameterizations to temperatures warmer than -37°C. Moreover, because deposition freezing is thought to be negligible in mixed-phase ~~clouds~~ conditions (e.g. Ansmann et al., 2008; DeMott et al., 2010; Hoose et al., 2008; Lohmann et al., 2016), the ice crystals are allowed to form only in the presence of cloud droplets, effectively changing the deposition freezing parameterizations into a type of condensation freezing. The maximum number of nucleated ice crystals by the modified Cooper (1986) (or, alternatively, Meyers et al., 1992) scheme is increased to 0.15 cm^{-3} s^{-1}. While these modifications aim to provide a more physically consistent representation of mixed-phase clouds, we did not explicitly evaluate the scheme's performance for this cloud type, as it lies outside the main scope of this study. A number of further refinements ~~to~~ would be necessary to achieve a more accurate simulation of mixed-phase clouds, as discussed ~~later~~ in section 5.1.

2.1.3 Modifications to ice nucleation: cirrus ice nucleation

As we limited the existing ice nucleation mechanisms to the mixed-phase regime (Sec. 2.1.2), we implement a new ice nucleation scheme for T<-37°C, which ~~also~~ helps mitigate the bias in ice crystal number concentration (ICNC; see also Sec. 5.1 for more detail). The newly implemented approach follows Shi et al. (2015) (Fig. 1b, labeled as cirrus nucleation) and represents the competition between homogeneous and heterogeneous nucleation in cirrus clouds (Liu and Penner, 2005) and the effect of pre-existing ice crystals. The scheme is fed by a predefined, temperature-dependent value of ice nucleating particles (INPs). In this work, the INP number is set to $2{\cdot}10^{-3}$ cm^{-3} at temperatures colder than -70°C and increases linearly to $20{\cdot}10^{-3}$ cm^{-3} at temperatures of -40°C and warmer. While the INP number in the upper troposphere is subjected to large uncertainties, the suggested numbers are plausible for relatively clean, aerosol-free environments in the tropical Pacific and follow model-simulated INP concentrations (Gasparini and Lohmann, 2016). The number of sulfate aerosols is set to 20 cm^{-3} and is thus not a limiting factor in ice nucleation.

2.1.4 Modifications to ice nucleation: ice crystal number limit

Very importantly, the maximum allowed ICNC is relaxed from a very limiting 0.5 to 20 cm^{-3}. Such high concentrations were occasionally observed in aircraft measurements of fresh anvils (Krämer et al., 2020; Jensen et al., 2018). Increasing the ICNC limit alone was previously shown to change anvil cloud properties, leading to more thin cirrus (e.g., Fig. 11a in Gasparini et al., 2019).

2.1.5 Other changes impacting cirrus

The cirrus nucleation scheme requires the input of an updraft velocity, and we choose to input the sum of the resolved vertical wind and an estimate of subgrid-scale updraft strength derived from the subgrid-scale turbulent kinetic energy (TKE_{SGS}) as $W_{TKE,SGS} = \sqrt{0.667 \cdot TKE_{SGS}}$, given that not all updrafts relevant for cloud formation are resolved at horizontal grid spacings of about 1 km (see more in Sec. 4.3). The $W_{TKE,SGS}$ term is computed assuming that the TKE_{SGS} ($TKE_{SGS} = 1/2 \cdot (u'u' + v'v' + w'w')$) is equally partitioned in the three directions ($w'w' = u'u' = v'v'$), and therefore $TKE_{SGS} = 3/2 \cdot w'w'$, where $W_{TKE,SGS} \equiv w'$.

~~Finally, we~~ We use a more accurate formulation for the saturation vapor pressure of liquid water and ice (Murphy and Koop, 2005), replacing the Flatau et al. (1992) formulation, which performs poorly at cold temperatures in the TTL. This change particularly affects in situ ice nucleation at temperatures below -70°C in the TTL (see Fig. 11 in Murphy and Koop, 2005).

Additionally, we adjust the homogeneous freezing threshold for cloud droplets from -40°C to -37°C. While droplets can freeze over a wide temperature range, larger droplets may freeze as warm as -35°C (Ickes et al., 2015; Shardt et al., 2022). Despite issues with using a fixed temperature freezing threshold (Herbert et al., 2015), -37°C is a more physically justified value than the -40°C used in the reference version of the P3 microphysical scheme.

2.1.6 Passive tracers

We implemented two passive tracers to facilitate the analysis of the tropical cirrus lifecycle. The "time after detrainment" or simply "detrainment" tracer, denoted A, evolves as:

$$A(\mathbf{x},t) = 1 \quad \text{where } |w| > 1\frac{m}{s},\ q_c + q_i > 10^{-6}\frac{kg}{kg},\text{ and } T'_\rho > 0 \tag{1}$$

$$\frac{\partial A}{\partial t} = -\frac{A}{\tau_A} \quad \text{elsewhere} \tag{2}$$

where w is the vertical ~~velocity~~wind, q_c and q_i the cloud liquid and ice mass mixing ratios, T'_ρ the density temperature anomaly from the domain mean (which is proportional to buoyancy), and $\tau_A = 80$ minutes is an arbitrary decay timescale for A, that allows for analysis of processes on timescales of hours to days. Neglecting the effects of subgrid-scale mixing on the passive tracer, A, the time since detrainment from active convection can be calculated as:

$$\tau_{detr} = -\tau_A \times log(A) \tag{3}$$

The behavior of the tracer in the context of idealized tropical convection is described in the appendix of Gasparini et al. (2022).

Additionally, we implement an analogous tracer to determine the time after in situ ice nucleation. The tracer is set to 1 in all grid cells with active cirrus ice nucleation and decays elsewhere with the same decay timescale τ_A. We note that both implemented tracers follow air parcels and not ice crystals, which results in biases when ice crystals sediment out of air parcels.

2.2 Simulation setup

We use a tropical channel setup that is wide in the zonal direction (3888 km) and narrow in the meridional direction (36 km) with double-periodic boundary conditions. The prescribed sea surface temperatures vary sinusoidally in the zonal direction between 24°C at the domain edge and 28°C in the middle of the domain. Convection develops over the warmer SSTs and gives rise to a large-scale overturning circulation in the zonal direction reminiscent of the Walker circulation. Such a "mock-Walker" circulation setup is therefore appropriate for studying the interplay between convection, clouds, and radiation in the tropics (Bretherton et al., 2006; Bretherton, 2007; Wing et al., 2023; Silvers et al., 2023). To accurately represent processes in the TTL, we impose a mean large-scale vertical ~~velocity~~ wind based on observations by Yang et al. (2008). Zonal winds increase linearly with altitude from 0 m s^{-1} at surface to 5 m s^{-1} at altitudes above 14 km. Our "mock-Walker" setup follows the one described in more detail by Blossey et al. (2010). The simulations are performed for 30 days, of which the last 20 are used for analysis.

2.3 In-situ observations~~of ice cloud properties and updraft velocities~~

For a fairer comparison with model data, which simulates a climate comparable to that of the tropical Pacific, we use airborne data from three campaigns in the tropical western Pacific: Airborne Tropical TRopopause EXperiment (ATTREX; Jensen et al., 2017); Pacific Oxidants, Sulfur, Ice, Dehydration, and cONvection experiment (POSIDON, Jensen et al., 2018); and the CONvective TRansport of Active Species in the Tropics (CONTRAST) ~~Experiment~~ experiment (Pan et al., 2017).

Vertical ~~velocity~~ wind data are only used from the tropical western Pacific flights of the ATTREX and POSIDON campaigns. The data are sampled using NASA's Meteorological Measurement System (MMS) instrument (Scott et al., 1990), which has a time resolution of 20 Hz. ~~The vertical velocity variance is computed at 1 Hz after the data has been~~ Vertical wind data is corrected by detrending and removing the mean of each flight leg. More details on the processing ~~of updraft velocities are~~ is described in Atlas and Bretherton (2023).

In situ data of ice cloud properties for the three campaigns is taken from the Krämer et al. (2020) dataset. The ~~data from the POSIDON and ATTREX field campaigns was recently corrected for a bug in the estimate of ICNC, which substantialy increased the ICNC. The~~ measurement resolution is 1 Hz, with an aircraft velocity of 170 m/s in POSIDON and ATTREX and 200 m/s in the CONTRAST campaign. The lower limit of detectable particle concentration in a given sampling time depends on the aircraft velocity and sampling area of the respective instrument (Krämer et al., 2020; Costa et al., 2017). This limits the measurements for CONTRAST of ice crystals at the ICNC <0.01 cm^{-3} and mean mass ice radii smaller than 35 μm. For consistency, model output under such conditions is not included in the calculation of model performance. Due to the slower aircraft speed and different instrumentation, there is no such limitation for POSIDON and ATTREX. The dataset contains ~~only few~~ limited measurements within or very near active deep convection (see Fig. A3).

2.4 Satellite retrievals

We use satellite retrievals from the years 2007-2010 for the tropical western Pacific (TWP) (20°S-20°N, 145°-180E°), an almost exclusively ocean-covered area characterized by persistent deep convection throughout the year. In the selected years, all the satellite products used have complete data coverage.

2.4.1 DARDAR

This dataset is derived from combined retrievals ~~by~~ from the CloudSat Cloud Profiling Radar (Stephens et al., 2008) and the Cloud-Aerosol Lidar with Orthogonal Polarization (CALIOP, Winker et al., 2010). Merged CloudSat radar reflectivity and CALIOP lidar attenuated backscatter signals were used to build the radar/lidar product (DARDAR, Delanoë and Hogan, 2008, 2010) that ~~retrieves~~ estimates ice water content (IWC), effective ice crystal size, and the extinction coefficient. DARDAR has a horizontal footprint of 1.7 km and a vertical resolution of 60 m. We only use the vertically integrated IWC, which includes all frozen hydrometeors and is denoted here as ice water path (IWP). Since the lidar signal is noisier during daytime, resulting in the detection of fewer thin clouds (Avery et al., 2012), we use nighttime-only data. While this may lead to a bias, the diurnal cycle of tropical oceanic convection is small and of second order importance for the comparison with model results (Wall et al., 2020; Gasparini et al., 2022). As one measure of uncertainty in the retrievals, IWP comparisons are made with both the newest dataset (DARDARv3) and an older version of the retrieval algorithm (DARDARv2) (Cazenave et al., 2019). IWP retrievals in DARDAR products are expected to reliably detect clouds down to an IWP of about 0.5 g m^{-2} (Sourdeval et al., 2016).

2.4.2 2C-ICE

We also use retrievals of IWP from the Cloudsat and CALIPSO Ice Cloud Property Product (2C-ICE) version RF05 (Deng et al., 2015). Despite originating from the same input data as the DARDAR product, ~~its ice properties are derived using different assumptions and therefore~~ analyzing it along with DARDAR helps quantify the uncertainty in satellite-retrieved quantities~~through comparisons with DARDAR nighttime-only data~~.

2.5 ~~Cloudsat-Calipso-CERES-MODIS (CCCM)~~

2.4.1 Cloudsat-Calipso-CERES-MODIS (CCCM)

The CALIPSO-CloudSat-CERES-MODIS (CCCM) dataset (Kato et al., 2011) merges cloud fraction data from CALIPSO lidar (Winker et al., 2010) and CloudSat radar (Stephens et al., 2008) with ~~MODIS~~ the Moderate Resolution Imaging Spectroradiometer

(MODIS) IWP data and ~~CERES~~ Clouds and the Earth's Radiant Energy System (CERES) radiative fluxes (Wielicki et al., 1996). MODIS IWP retrievals are unreliable for detection of thin cirrus (IWP smaller than about 4 g m^{-2}, Sourdeval et al., 2016). CCCM's horizontal resolution is about 30 km, equivalent to CERES retrievals. Shortwave (SW) radiative fluxes from CERES used in this work are from the measured fluxes during the 1:30 pm satellite overpass, accounting for diurnally averaged insolation values. Data points with zenith angles greater than 70° are excluded to mitigate issues at high solar zenith angles. Albedo is computed based on incoming and outgoing SW fluxes at the top of the atmosphere (TOA). The average reflected SW flux during the day is calculated by multiplying the albedo by the daily and yearly average incoming radiation, set at 409.6 W m^{-2}, the annual average insolation for the band between 20°S and 20°N (Wing et al., 2018). This ensures that values of radiative fluxes are comparable to the climatological cloud radiative effects.

The TOA albedo (α) and SW cloud radiative effect (CRE) are computed as

$$\alpha = \frac{SW_{out}}{SW_{in}} \tag{4}$$

$$SW_{CRE} = -(\alpha - \alpha_{clear-sky}) \times 409.6 W m^{-2} \tag{5}$$

In addition, Fig. B2 compares model computed quantities with directly retrieved radiative fluxes to ensure better consistency with retrievals. SW CRE is thus computed as

$$SW_{CRE} = -(SW_{out} - SW_{out,clear-sky}) \tag{6}$$

The LW CRE is computed as

$$LW_{CRE} = -(OLR_{clear-sky} - OLR_{clear-sky}) \tag{7}$$

where OLR is outgoing LW radiation at the TOA.

2.5 Global storm resolving models from DYAMOND-1

We compare the power spectral density of vertical wind between SAM and four global storm resolving models (GSRMs) in Sec. 4.5. GSRM simulations were run with the Nonhydrostatic ICosahedral Atmospheric Model (NICAM), Global System for Atmospheric Modeling (gSAM), Finite Volume Cubed-Sphere Dynamical Core (FV3), and Icosahedral Nonhydrostatic Weather and Climate Model (ICON), as part of the DYAMOND-1 experiment (Stevens et al., 2019). The GSRM simulations have horizontal grid spacings of 2.5-5 km and vertical grid spacings of 400-500 m. Vertical winds are analyzed within a square swath in the tropical western Pacific (4°S-4°N, 144°-152°E), a region overlapping the aircraft measurements with a comparable climatology to the SAM simulations. Vertical winds are analyzed for model levels closest to 14.2 km, the most common height for ATTREX level leg sampling.

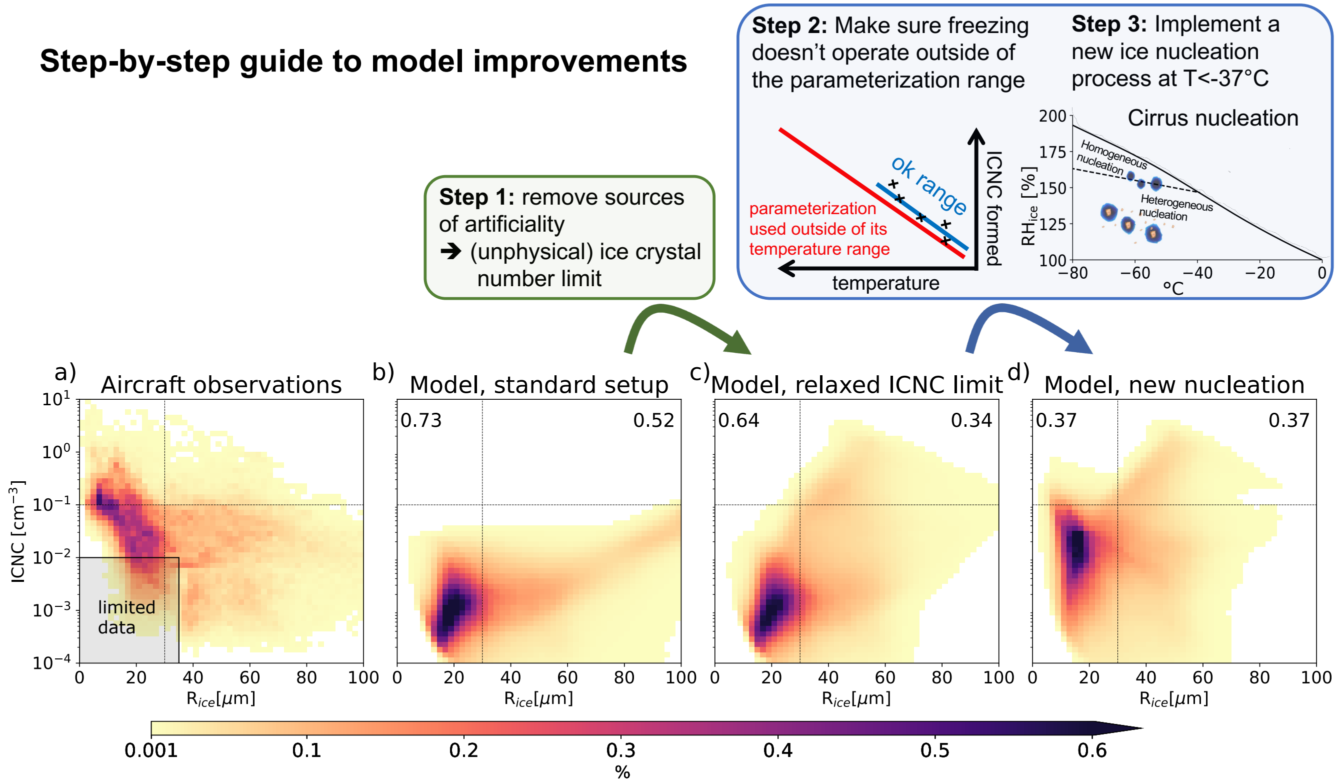

Figure 2. Probability density function of ice properties for clouds at T<-40°C as a function of ICNC and ice mass radius (computed as the radius of a solid ice sphere with mass IWC/ICNC, as in Krämer et al., 2020) for (a) ~~A simulated mesoscale convective system with an extensive anvil cloud shield~~ tropical Pacific aircraft observations and ~~overlying TTL cirrus. Purple contours in a~~three versions of the SAM model: (b) ~~indicate rain~~the standard setup (Sec. ~~Panels b~~2.1.1)~~and~~, (c) ~~show values of detrainment and in-situ nucleation tracers for~~ the ~~same cloud system~~intermediate model version with a relaxed ICNC limit (Sec. ~~Panel~~ 2.1.4), and (d) ~~presents~~ the ~~outcome of~~ final version with a ~~cirrus origin classification criterion. In situ cirrus~~ modified ice nucleation scheme (including also improvements described in ~~orange~~Sections 2.1.2, 2.1.3, and 2.1.5)~~are defined as cloudy parcels that have not been~~. The numbers in ~~contact with detrained air for at least 30 hours and where~~ the ~~time since in situ nucleation tracer is shorter~~ upper left and right corner represent a 2D total variation distance of model data compared to ~~the time since detrainment. The remaining clouds are classified as anvil cirrus~~ aircraft observations (~~blue). Portions of~~ the ~~anvil where~~ smaller the ~~time since in situ nucleation tracer is shorter compared to~~ number, the ~~time since detrainment are classified as "dual-origin" (in brown~~better the agreement)~~. Gray contours delineate updraft velocities of 1~~, calculated separately for small (1-30 μm~~s^{-1}. Red contours in b~~) and ~~c~~large particle sizes (30-120 μm)~~delineate total cloud condensate of 1·10^{-4}gkg^{-1}~~. Observations are limited or not available in the shaded area.

3 Cirrus properties

3.1 Simulated tropical cirrus cloud properties and their comparison with aircraft observations and satellite retrievals

This section first outlines the step-by-step changes implemented in the ice microphysics scheme. We focus on changes under cirrus conditions, limiting the analysis to temperatures colder than -40°C and ice water contents larger than 10^{-5} g m^{-3}, which is close to the detectability threshold of the aircraft observations. The data are first presented in the ICNC–ice crystal mean mass radius (from now on: ice number–radius) space, which provides an intuitive aggregated perspective on ice cloud properties (Krämer et al., 2016; Gasparini et al., 2018).

Aircraft observations in Fig. 2a show a peak ICNC between 1 and 10^{-2} cm^{-3} for particles with mean mass radii smaller than 30 μm. For concentrations smaller than 10^{-1} cm^{-3}, the observed particle size often exceeds 50 μm. We note that due to retrieval limits, there are limited measurements available for ice radii smaller than 35 μm at number concentrations below about 10^{-2} cm^{-3} (see Methods).

The standard version of the SAM model coupled with the P3 scheme (Fig. 2b, Sec 2.1.1) is strongly biased compared to observations. Most notably, the model drastically underestimates ICNC as it lacks concentrations larger than $3{\cdot}10^{-2}$ cm^{-3}. We resolve a large part of the bias by implementing three key changes to the ice microphysics.

We first relax the maximum ICNC limit from $5{\cdot}10^{-2}$ cm^{-3} to 20 cm^{-3} (Fig. 2c, Sec. 2.1.4). This improves particularly the representation of particles larger than 30 μm, reducing the total variation distance metric (Gibbs and Su, 2002, a 2D analog to the root mean from 0.52 to 0.35. However, the model still strongly underestimates the number densities of small ice crystals in the top left quadrant, indicating errors in parameterizing ice formation under cirrus conditions.

The second key modification addresses the deposition freezing parameterization, which was incorrectly active at temperatures both below and above the homogeneous freezing threshold. Originally calibrated for temperatures warmer than -25°C (Fig. 1), this parameterization extended far beyond its intended range. We restrict it to T>-37°C and introduce a scheme to account for competition between homogeneous and heterogeneous nucleation at T<-37°C (Liu and Penner, 2005; Shi et al., 2015) (Sec. 2.1.2, 2.1.3). We also include a number of small changes to the microphysics, described in Sec. 2.1.5).

These changes cut the microphysical bias in half, improving the representation of both small and large particles (Fig. 2d). Nevertheless, some biases remain. The model continues to underestimate ICNC for small ice crystals and overestimate ICNC for larger crystals. These remaining biases largely originate from persistent challenges in representing ice microphysics (see Sec. 5.1) and from too low vertical wind variance in the model (see Sec. 4.5).

To provide an alternative perspective, we examine the model's performance by sorting results by temperature. The exponential decrease in IWC with decreasing temperature has improved compared to the standard model version and is well represented by the model (Fig. 3a-c). Observed ICNC shows large variability, but only a small change in the median number concentration with temperature (Fig. 3d). The model reproduces the observed median and spread, improving the agreement substantially compared to the standard model version (only the gray median is shown). Notably, the model still misses some of the (rather infrequent) high ICNC data points at cold temperatures.

Similarly to IWC, the mean mass radius decreases with temperature, with medians ranging from 80 μm at -40°C to 15 μm at -80°C. The model simulates particles that are too small at warmer temperatures (between -65°C and -40°C) and comparable to observations for T <-65°C. Notably, the spread in simulated particle size is narrower than observed, possibly due to the too simple single-mode description of ice microphysics (see Sec. 5.1).

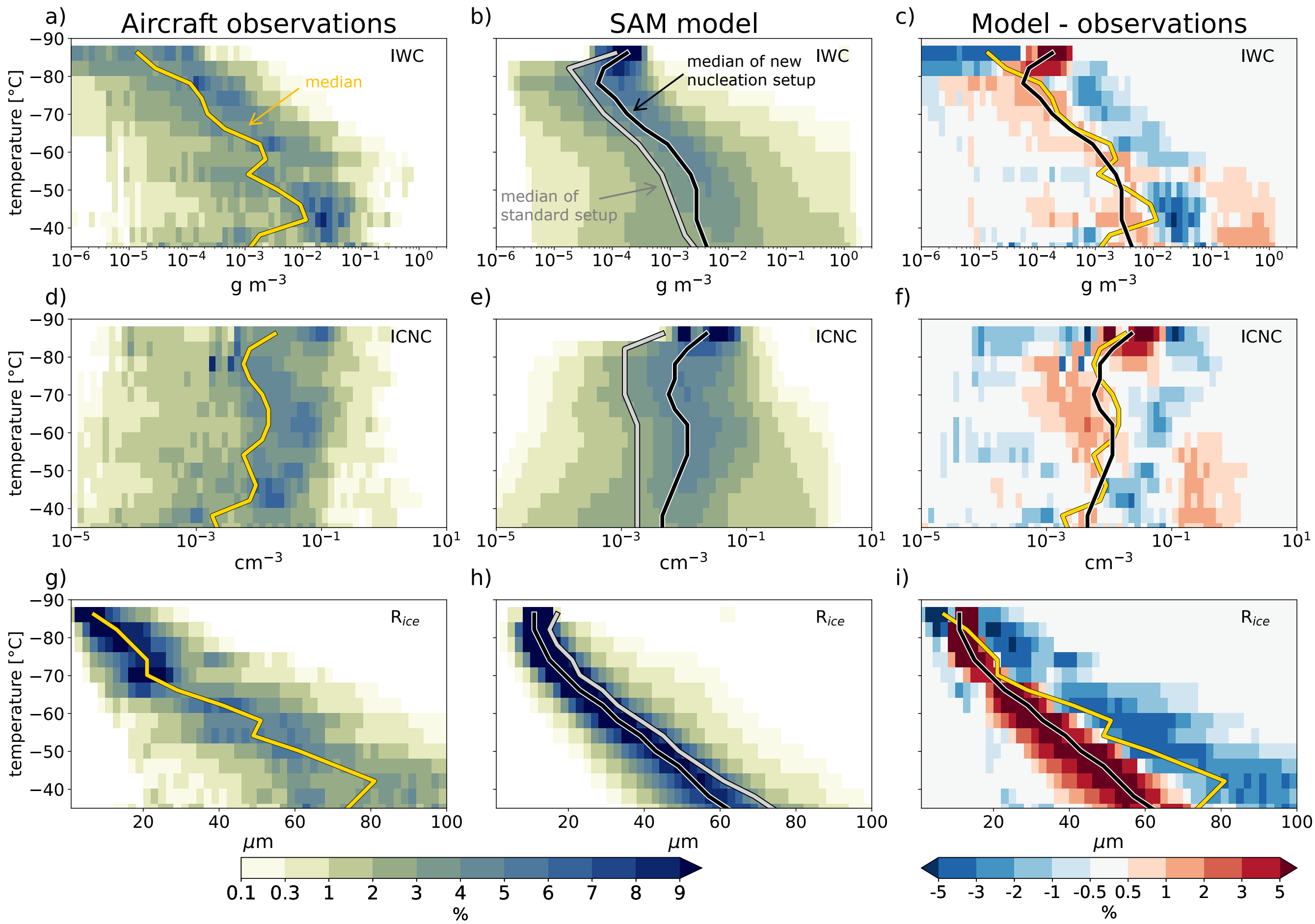

Figure 3. Cirrus cloud properties in tropical aircraft measurements (first column) and SAM model simulations with improved microphysics at 1 km horizontal grid spacing (second column). Lines represent median values. Gray lines in the middle column represent median values of the standard model setup. The third column shows the anomalies between SAM and aircraft data; the lines are copies of the lines on the first and second column panels. The data is sorted into 4°C temperature bins. The values in each temperature bin add up to 100%.

In summary, the temperature-sorted model results offer a complementary perspective on cirrus cloud properties, showing generally a good agreement with observations, while also highlighting persistent biases in ICNC at colder temperatures and particle size at warmer temperatures. Nevertheless, this agreement represents a substantial improvement compared with the earlier model version (Fig. 2), emphasizing processes where further refinement is still needed. The addition of passive tracers discussed in Section 4 helps pinpoint processes requiring further refinement, particularly the representation of in situ ice nucleation at cold temperatures.

3.2 The relevance of tropical cirrus for top-of-the-atmosphere radiative fluxes

To link cirrus cloud properties to the TOA radiative budget, we take an integrated perspective and categorize cloud occurrence frequency and radiative effects based on IWP. We neglect infrequent scenes with low clouds underlying thin cirrus, where low clouds are expected to dominate the CRE signal. Figure 4a compares the simulated IWP distribution with four satellite-derived datasets, showing that the improved model generally falls within or near the observed range. The apparent overrepresentation of the thinnest cirrus in the model and the corresponding slight underestimation of other cloud types in the normalized PDF should not be interpreted as a bias, as satellite retrievals are known to underestimate the thinnest cirrus clouds (Balmes and Fu, 2018; Lesigne et al., . Thin cirrus with IWP < 1 g m^{-2} make up 52% of all simulated cirrus but contribute only 6% to the LW CRE and 5% to the SW CRE, indicating that their direct radiative impact at the TOA is modest despite their frequency. Focusing on clouds with IWP > 1 g m^{-2}, which have a greater radiative influence, improves the model's agreement with satellite observations (Fig. B1).

Figure 4b shows the averaged CRE for high clouds in each IWP bin. The most frequent anvils according to satellite datasets occur at an IWP of 3-30 g m^{-2}, which corresponds to anvil clouds of intermediate optical depth (1-3) that yield a net positive, LW-dominated CRE (Sokol and Hartmann, 2020). For thicker clouds (IWP > 100 g m^{-2}), both model and satellite data show a dominance of SW CRE, with net CRE exceeding -100 W m^{-2} for the thickest anvils. However, the model overestimates the SW CRE, a bias partially resolved by averaging the output onto coarser grid scales, similar to the CERES pixel data resolution (36$\times$36 km grid boxes). Additionally, a recently identified bug in the ice optics parameterization likely increased the optical depth and radiative effects per unit IWP by $\sim$15%, but this issue could not be addressed in the current simulations. This SW bias becomes even more apparent when comparing CERES CRE retrieved during daytime satellite overpasses with model-simulated CRE between 1 and 2 pm local time (Fig. B2b).

Determining which type of tropical cirrus is radiatively most important is not straightforward. Are the less frequent but thick deep convective cores and fresh anvils, which have a strong influence on both SW and LW CRE, the most dominant, or do the more widespread anvil clouds of intermediate thickness dominate? Figure 4c provides an answer by scaling the CRE in a given IWP bin by that bin's frequency of occurrence: the radiatively most dominant clouds have IWP between 1 and 3000 g m^{-2}, similar to results by Berry and Mace (2014). These include anvil clouds with optical depths greater than approximately 1. Nonetheless, thinner cirrus (IWP 0.3–10 g m^{-2}, Fig. 4c) also contribute meaningfully to the net CRE, underscoring the importance of studying not only the thickest tropical cirrus but also their continued evolution until they reach an IWP of

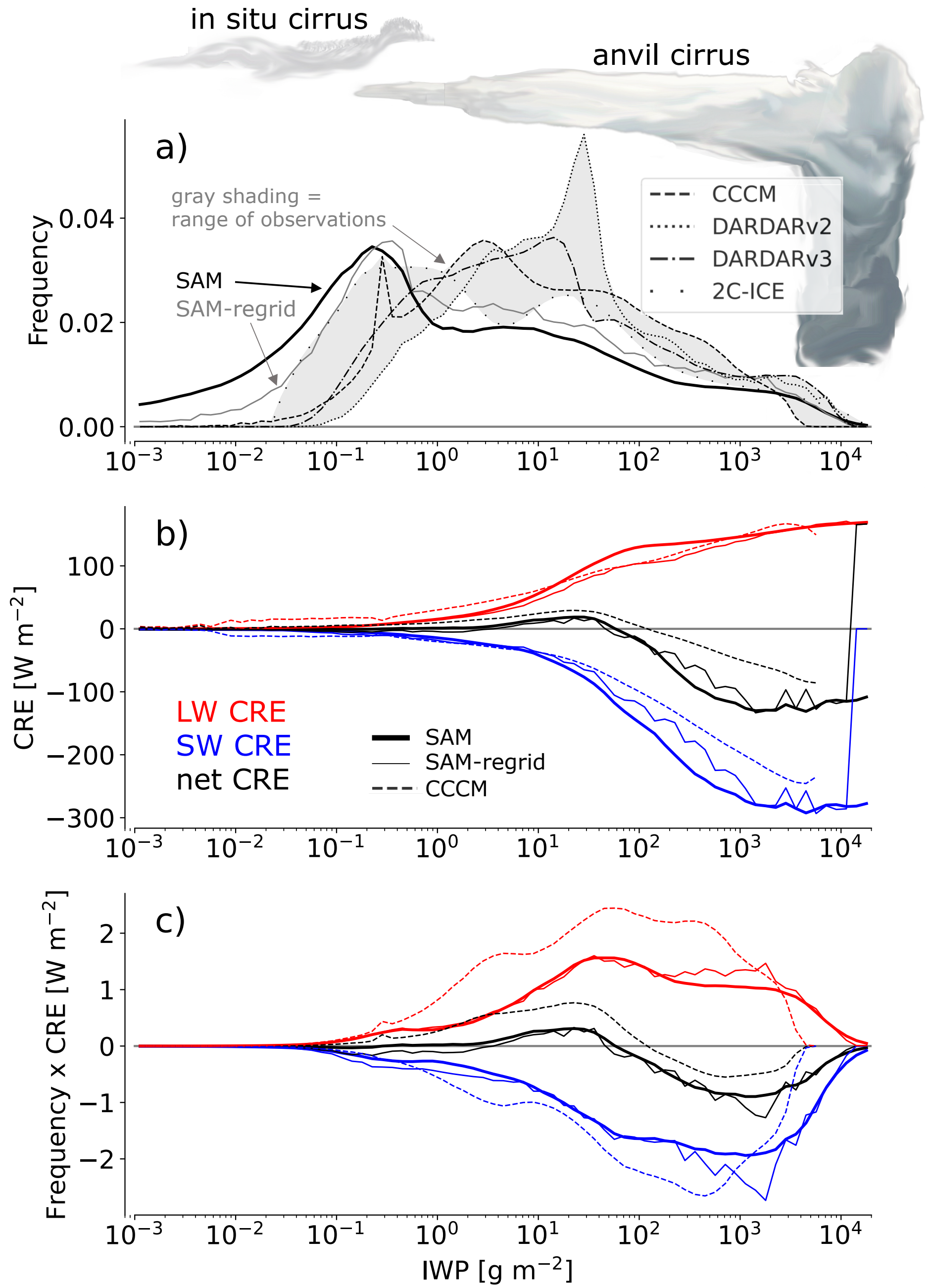

Figure 4. (a) Frequency of cloud occurrence in each ice water path (IWP) bin, (b) average CRE in each IWP bin, and (c) the contribution of each IWP bin to the CRE. The gray shading in panel a) highlights the range of observations. Panels b) and c) show results only for the improved SAM model and the CCCM satellite product. Model results are presented for full resolution and regridded to 36×36 km grid, similar to the resolution of CERES satellite retrievals of CRE.

$\sim$0.1 g m^{-2} (optical depth $\sim$0.005). Additionally, the response of thin cirrus to global warming remains highly uncertain (Sokol et al., 2024), and deserves further investigation.

4 Origin and evolution of cirrus

4.1 Cirrus origin

~~We use a case study and statistical estimates of cirrus origin to demonstrate~~

We illustrate the utility of passive tracers in disentangling ~~the contributions of~~ convective and in situ ~~processes~~ contributions to cirrus formation using a case study and statistical estimates of cirrus origin in the SAM model ~~with the improved microphysical scheme~~ that includes all model improvements (Sec. 2.1.2-2.1.5) and the two passive tracers (Sec. ~~??). Figure ??~~ 2.1.6). Our analysis begins with the model snapshot in Fig. 5, while a supplementary video shows the system's evolution over two days. The figure depicts a snapshot of a multicore mesoscale convective system with an anvil cloud shield extending approximately 500 km. This system includes a fresh, thick precipitating anvil cloud that evolves into a thinner, aged anvil cloud. Above this, a thin cirrus layer spans altitudes of 15–16 km. Identifying the origin of such thin cirrus from a single model output timestep is challenging. Although thin TTL clouds are typically formed in situ (Krämer et al., 2016; Huang and Dinh, 2022), they might also be remnants of TTL-penetrating deep convection.

Passive tracers resolve this uncertainty. The detrainment tracer highlights regions of active deep convection and thick anvil clouds with times since detrainment typically less than ten hours and reveals that the overlying thin cirrus resides predominantly in air undisturbed by convection for at least ~~30~~ 24 hours (Fig. ~~??~~5b). The in situ nucleation tracer confirms this, showing that much of the thin cirrus originates from recent ice nucleation events (within the last 5 hours; Fig. ~~??~~5c).

Interestingly, the nucleation tracer also indicates that some parts of the anvils experience ongoing ice nucleation. These events, driven by convective gravity waves or within-anvil updrafts, align with previous observational studies (Jensen et al., 2009; Hartmann et al., 2018; Krämer et al., 2020; Sokol and Hartmann, 2020). However, their broader significance for tropical cirrus remains uncertain (Dinh et al., 2023; Gasparini et al., 2023).

To better characterize the microphysical origin of cirrus, we classify them into three categories: ~~pure~~ in situ, anvil, and dual-origin. Anvil cirrus are defined as clouds where the time since detrainment is shorter than the time since in situ nucleation. ~~Pure in~~ In situ cirrus are those ~~not detrained~~ that have not experienced detrainment for at least ~~30 hours ,~~ 24 hours and where the time since nucleation is shorter ~~. The dual-origin category includes anvils clouds that are additionally influenced by~~ than the time since detrainment.

Dual-origin cirrus are clouds detrained within the last 24 hours that have a shorter time since in situ nucleation ~~within or at anvil edge or cirrus forming near~~ compared to time after detrainment. These typically form within or near anvils or in cirrus clouds close to active convection (Fig.~~??~~5d). ~~Notably, while~~ To correct for classification biases due to ice crystal sedimentation impacting older anvils and in situ cirrus, clouds that were initially classified as in situ cirrus but located below dual-origin cirrus are ~~affected~~ reassigned to the dual-origin category. Although dual-origin cirrus are influenced by in situ nucleation, their total ice mass and number ~~remain~~ are still dominated by convective outflow (not shown).

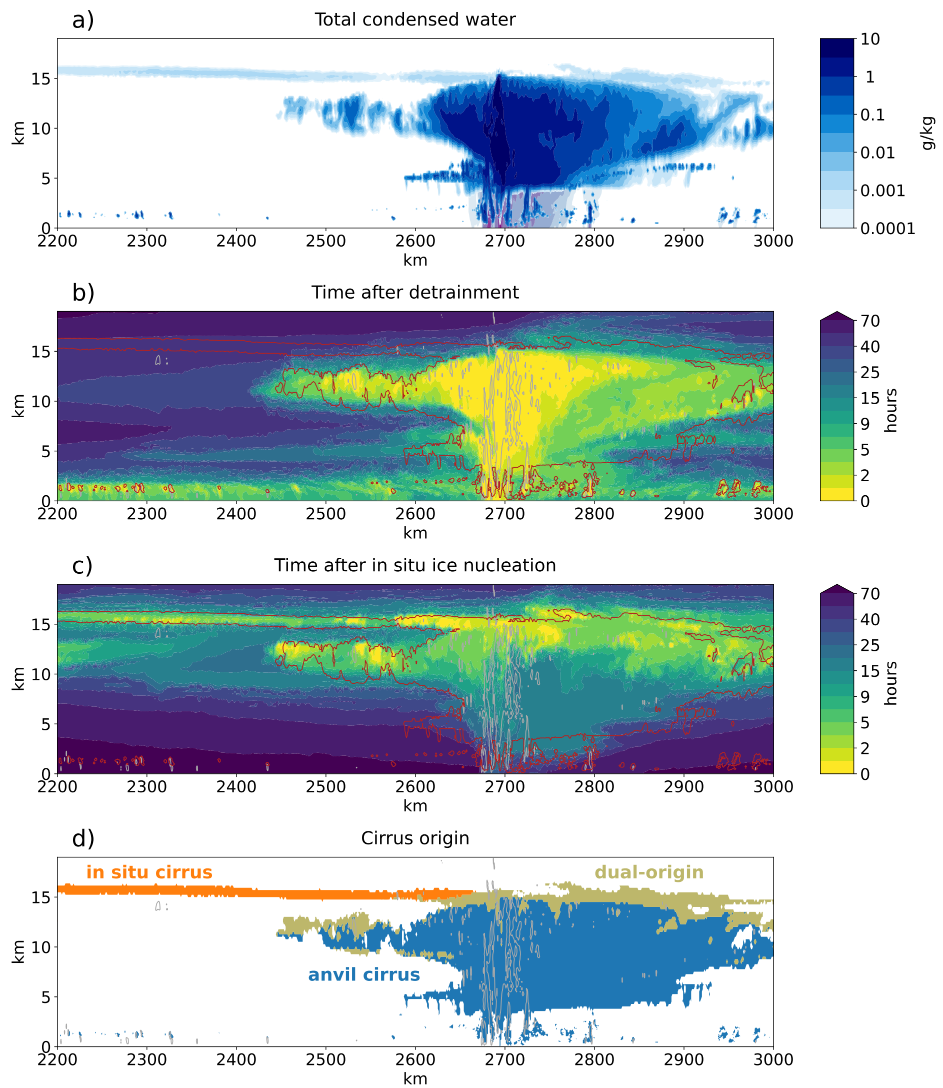

Figure 5. A simulated mesoscale convective system with an extensive anvil cloud shield and overlying TTL cirrus. Panel a) shows total condensed water, with purple contours indicating rain. Panels b) and c) show values of detrainment and in-situ nucleation tracers for the same cloud system, respectively. Panel d) presents the outcome of a cirrus origin classification criterion. In situ cirrus (in orange) are defined as cloudy parcels that have not been in contact with detrained air for at least 24 hours and where the time since in situ nucleation tracer is shorter compared to the time since detrainment. The remaining clouds are classified as anvil cirrus (blue). Portions of the anvil where the time since in situ nucleation tracer is shorter compared to the time since detrainment are classified as "dual-origin" (in brown). Gray contours in b), c) and d) delineate vertical wind velocities of 1 m s^{-1}. Red contours in b) and c) delineate total cloud condensate of $1 \cdot 10^{-4} gkg^{-1}$.

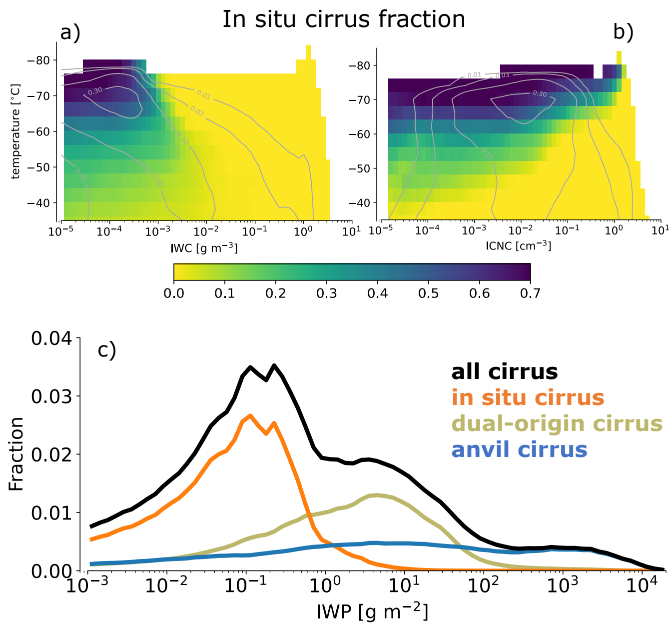

Figure 6. Fraction of in situ cirrus represented in the (a) temperature-IWC and (b) temperature-ICNC space for the cirrus classification criterion from Fig. ~~??~~5. The gray lines in the contour indicate the joint distribution of cloud occurrence in each two-dimensional phase space. Panel c) shows the fraction of cirrus binned by IWP.

Our tracer approach confirms previous findings highlighting IWC as a good predictor of cirrus origin (Krämer et al., 2016). High-IWC tropical cirrus are thought to be of convective origin, while low-IWC cirrus, particularly those at cold temperatures, are more likely of in situ origin (Luebke et al., 2016; Krämer et al., 2016). Using a two-dimensional IWC-temperature space, we find that in situ cirrus dominate only for the coldest, low IWC tropical cirrus (IWC $< 10^{-3}$ g m^{-3}, T $<$ ~~-70~~-65°C), while high-IWC cirrus and most cirrus at warmer temperatures are of convective origin (Fig. 6a). In situ contributions range from 10% (T $>$ -50°C) to ~~50~~more than 70% (T $<$ -70°C)~~, an estimate that is likely a lower bound because it excludes portions of the dual-origin category that could be considered in situ cirrus. Additionaly~~. Additionally, we repeat the analysis using ICNC, which leads to less distinct patterns (Fig. ~~??~~6b). While ~~high~~ the highest ICNC bins are clearly associated with anvil cirrus, in situ cirrus fractions remain steady at ∼~~20~~10–40% for ICNC $<$ 0.03 cm^{-3}, increasing to over ~~50~~60% only at temperatures colder than ~~-60~~-65°C.

~~Finally, vertically~~ Vertically integrated cirrus origin analysis in Fig. ~~??~~6c shows that in situ cirrus dominate at IWP $<$ 0.4 g m^{-2} and peak at IWP values between 0.1 and 0.5 g m^{-2}. At IWP $>$ 10 g m^{-2}, in situ nucleation is highly unlikely due to limited vapor availability and slow depositional growth in the TTL. Clouds with IWPs of 1–~~10~~ 50 g m^{-2} often consist of contributions from both in situ and convective sources, suggesting that in situ nucleation plays a role in sustaining and prolonging ~~aged cirrus lifetime~~the lifetime of aged anvil clouds. This analysis, together with our previous findings (Fig. 6), provides more information about the evolution of tropical cirrus. These can be split into two separate evolution pathways, as qualitatively depicted in Fig. 4a. Thick anvils originating in high IWP deep convective towers spread and thin towards IWP $\sim$1 g m^{-2}, while thinner cirrus (IWP $<$ 1 g m^{-2}) predominantly form via in situ ice nucleation. And while ice nucleation is very frequent and may play an important role in prolonging anvil lifetime (Hartmann et al., 2018), dual-origin cirrus generally preserve convective-like properties and could, for simplicity, be merged with the anvil category.

4.2 Radiative importance of tropical cirrus based on their origin

Type of cirrus	LW CRE [W/m^2] (Fraction of total)	SW CRE [W/m^2] (Fraction of total)	NET CRE [W/m^2] (Fraction of total)
Anvil cirrus	20.1 (53.0%)	-27.7 (62.2%)	-7.6 (115.2%)
Dual-origin cirrus	16.1 (39.8%)	-13.9 (31.1%)	1.2 (-18.5%)
In situ cirrus	2.7 (7.2%)	-2.9 (6.6%)	-0.2 (3.3%)

Table 1. Cloud radiative effects (CRE) for cirrus types and their respective relative importance (in parentheses).

Finally, by multiplying the cloud occurrence frequency in Fig. 6c with the IWP-binned CRE in Fig. 4b we estimate the radiative contribution of each of the three cirrus types, summarized in Table 1. Anvil clouds are radiatively most important, accounting for more than 50% of both LW and SW CRE of all tropical cirrus. They dominate in the high IWP range, where SW CRE is stronger than LW CRE, leading to a net CRE of about -8 W m^{-2}. Dual-origin cirrus are aged anvils that dominate moderate IWP. They are still radiatively very important, leading to 40% of the total LW and 30% of the total SW CRE. Finally, in situ cirrus radiative contribution accounts only for 7% of the total LW and SW CRE. The estimate of their SW CRE may be biased high due to the occurence of lower-lying anvils or dual-origin clouds, likely leading to an overestimation of the SW CRE. A more detailed radiative analysis accounting for cloud overlap (see e.g., Deutloff et al., 2025) is left for future work.

4.3 Evolution of tropical cirrus

The two passive tracers provide new insights into the distinct microphysical evolution pathways of detrained anvils and in situ cirrus. ~~The tracer data are presented in the ICNC–ice crystal mean mass radius (from now on: ice number–radius) space (Fig. ??), which provides an intuitive aggregated perspective on ice cloud properties, and has been used already in the analysis of observational and model data (Krämer et al., 2016; Gasparini et al., 2018).~~ This perspective helps differentiate and track the lifecycle of numerous cirrus clouds formed in our simulation, offering a more comprehensive understanding of cirrus evolution compared to a snapshot perspective.

For detrained anvils, deep convection initially injects high concentrations (ICNC $>$ 0.1 cm^{-3}) of ice crystals spanning a broad size range, including relatively large particles (Fig. 7b). The tracers allow for the study of how these crystals evolve

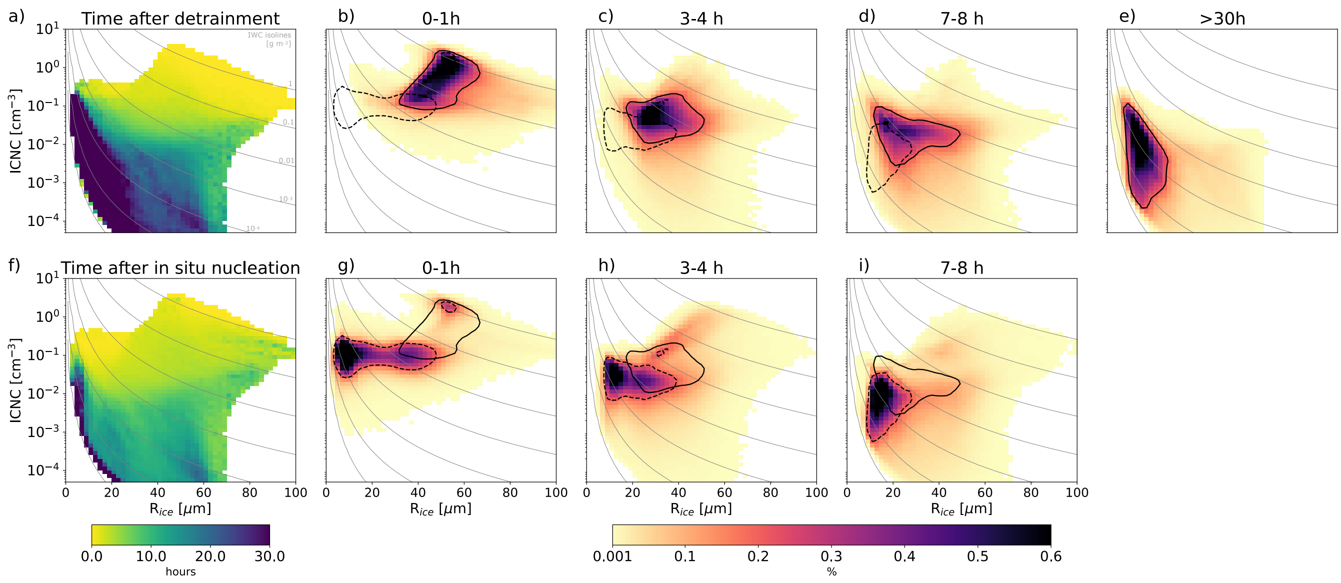

Figure 7. Evolution of microphysical properties tracked with passive tracers~~as a function of ICNC and ice mass radius (computed as the radius of a solid ice sphere with mass IWC/ICNC, as in Krämer et al., 2020)~~. Panels a) and f) represent the mean time of air parcels after detrainment and in situ nucleation. The other panels present the joint distribution of ICNC and mass radius for the stated time after detrainment (upper row) or time after in situ ice nucleation (lower row). The two contour lines encircle the peak probability distribution of particles under the selected conditions (detrainment = solid lines; nucleation = dashed lines). Isolines of IWC are plotted in gray. Since there are very few grid boxes at time after in situ nucleation of more than 30 h, we omit that panel.

over time: within the first 1–3 hours following detrainment, there is a rapid decrease of both number concentration and size due to sedimentation, marking the most dynamic phase of anvil evolution (compare Fig. ~~??~~7b and c). Beyond this period, the evolution slows, with ice mass and number decreasing gradually as sedimentation and sublimation deplete the ice crystals (compare Fig. ~~??~~7c and d). Panel ~~??~~7e shows properties of clouds classified as in situ cirrus in Figs. ~~??d and ??~~5d and 6.

In contrast, freshly nucleated in situ cirrus ice crystals form at smaller sizes and intermediate concentrations (ICNC: 0.02–0.2 cm^{-3}). Homogeneous nucleation events occasionally spike these concentrations but remain transient and thus are barely visible in our frequency figure. Since most of the in situ crystals are smaller than ~~30 μm~~the freshly detrained ones (Fig. 7 g-i), sublimation may be a more important ice crystal sink than sedimentation. This may imply a greater sensitivity to atmospheric thermodynamic conditions, such as temperature and supersaturation fluctuations. Over time, in situ cirrus ~~also~~ tend to lose ice number and size, ~~eventually converging to microphysical properties comparable to~~ approaching microphysical properties that often overlap with those of aged anvil cirrus. In summary, while both in situ and detrained cirrus retain distinct properties in the first 3–5 hours, they become harder to distinguish in the later stages of their evolution.

4.4 Simulated tropical cirrus cloud properties and their comparison with aircraft observations and satellite retrievals

Probability density function of ice properties for clouds at T<-40°C for (a) tropical Pacific aircraft observations and three versions of the SAM model: (b) the standard setup, (c) the intermediate model version with a relaxed ICNC limit, and (d) the final version with a modified ice nucleation scheme. The number represents a 2D total variation distance of model data compared to aircraft observations (the smaller the number, the better the agreement), calculated separately for small and large particle sizes. Observations are limited or not available in the shaded area.

This section first outlines the step-by-step changes implemented in the ice microphysics scheme in the ice number–radius space. We focus on changes under cirrus conditions, limiting the analysis to temperatures colder than -40°C and ice water contents larger than 10^{-5} g m^{-3}, which is close to the detectability threshold of the aircraft observations.

Aircraft observations in Fig. 2a show a peak ICNC between 1 and 10^{-2} cm^{-3} and mean mass radii smaller than 30 μm. The mode extends to 3 cm^{-3} at particle sizes smaller than 20 μm. Moreover, for concentrations smaller than 10^{-1} cm^{-3}, the observed particle size often exceeds 50 μm. We note that due to retrieval limits, there are no measurements available for ice radii smaller than 35 μm at number concentrations below about 10^{-2} cm^{-3} (see Methods).

The standard version of the SAM model coupled with the P3 scheme (Fig. 2b) is strongly biased compared to observations. Most notably, the model drastically underestimates ICNC as it lacks concentrations larger than 10^{-2} cm^{-3}. We resolve a large part of the bias by implementing three key changes to the ice microphysics.

We first relax the maximum ICNC limit from $5{\cdot}10^{-2}$ cm^{-3} to 20 cm^{-3} (Fig. 2c). This improves the representation of particles larger than 30 μm, reducing the total variation distance metric (Gibbs and Su, 2002, , a 2D analog to the root mean square error) from 0.52 to 0.35. However, the model still strongly underestimates the number densities of small ice crystals, indicating errors in parameterizing ice formation under cirrus conditions.

The second modification addresses the deposition freezing parameterization, which was incorrectly active at temperatures both below and above the homogeneous freezing threshold. Originally calibrated for temperatures warmer than -25°C (Fig. 1), this parameterization extended far beyond its intended range. We restrict it to T>-37°C and introduce a scheme to account for competition between homogeneous and heterogeneous nucleation at T<-37°C (Liu and Penner, 2005; Shi et al., 2015). This scheme captures low ICNC heterogeneous nucleation at RH$_{ice}$ > 120% while also allowing for homogeneous nucleation events under sufficiently strong updrafts and high RH$_{ice}$.

The two changes cut the microphysical bias in half, improving the representation of both small and large particles (Fig. 2d). Nevertheless, some substantial biases remain. The model continues to underestimate ICNC for small ice crystals and overestimate ICNC for larger crystals that represent freshly detrained particles (Fig. **??**a-b). These remaining biases largely stem from persistent challenges in representing ice microphysics (see Discussion) and from too low vertical wind variance in the model (see Section 4.3).

Cirrus cloud properties in tropical aircraft measurements (first column) and SAM model simulations with improved microphysics at 1 km horizontal grid spacing (second column). Lines represent median values. Gray lines in the middle column represent median values of the standard model setup. The third column shows the anomalies between SAM and aircraft data; the lines are copies of the lines on the first and second column panels. The data is sorted into 4°C temperature bins. The values in each temperature bin add up to 100%.

To provide an alternative perspective, we examine the model's performance by sorting results by temperature. The exponential decrease in IWC with decreasing temperature, as expected from the Clausius-Clapeyron relationship, has improved compared to the standard model version and is well represented by the model (Fig. **??**a-c). Observed ICNC shows large variability, with more than one order of magnitude increase in the median number between temperatures of -40°C and -70°C (Fig. **??**d). The model reproduces the observed median and spread for temperatures warmer than -65°C but underestimates ICNC at the coldest temperatures, although this bias has been substantially improved compared to the standard model version (only gray median shown). This bias aligns with the underrepresentation of small particles highlighted in Fig. 2. Insights from tracers (Fig. **??**) suggest the bias may stem from too few in situ nucleated particles or insufficient detrainment of small particles from deep convection.

Similarly to IWC, the mean mass radius decreases with temperature, with medians ranging from 80 μm at -40°C to 15 μm at -80°C. The model simulates particles that are too small at warmer temperatures (between -55°C and -40°C) and slightly too large at T <-70°C. Notably, the spread in simulated particle size is narrower than observed, possibly due to the too simple single-mode description of ice microphysics (see Discussion).

In summary, the temperature-sorted model results offer a complementary perspective on cirrus cloud properties, showing good agreement with observations for temperatures warmer than -60°C while highlighting persistent biases at colder temperatures. Nevertheless, this agreement represents a substantial improvement compared with the earlier model version (Fig. 2), emphasizing processes where further refinement is still needed. The addition of passive tracers discussed in section 3 helps pinpoint processes requiring further refinement, particularly the representation of in situ ice nucleation at cold temperatures.

Horizontal grid spacing dependence]Cirrus properties

4.4 Simulated tropical cirrus cloud properties and their comparison with aircraft observations and satellite retrievals

Probability density function of ice properties for clouds at T<-40°C for (a) tropical Pacific aircraft observations and three versions of the SAM model: (b) the standard setup, (c) the intermediate model version with a relaxed ICNC limit, and (d) the final version with a modified ice nucleation scheme. The number represents a 2D total variation distance of model data compared to aircraft observations (the smaller the number, the better the agreement), calculated separately for small and large particle sizes. Observations are limited or not available in the shaded area.

This section first outlines the step-by-step changes implemented in the ice microphysics scheme in the ice number–radius space. We focus on changes under cirrus conditions, limiting the analysis to temperatures colder than -40°C and ice water contents larger than 10^{-5} g m^{-3}, which is close to the detectability threshold of the aircraft observations.

Aircraft observations in Fig. 2a show a peak ICNC between 1 and 10^{-2} cm^{-3} and mean mass radii smaller than 30 μm. The mode extends to 3 cm^{-3} at particle sizes smaller than 20 μm. Moreover, for concentrations smaller than 10^{-1} cm^{-3}, the observed particle size often exceeds 50 μm. We note that due to retrieval limits, there are no measurements available for ice radii smaller than 35 μm at number concentrations below about 10^{-2} cm^{-3} (see Methods).

The standard version of the SAM model coupled with the P3 scheme (Fig. 2b) is strongly biased compared to observations. Most notably, the model drastically underestimates ICNC as it lacks concentrations larger than 10^{-2} cm^{-3}. We resolve a large part of the bias by implementing three key changes to the ice microphysics.

We first relax the maximum ICNC limit from $5{\cdot}10^{-2}$ cm^{-3} to 20 cm^{-3} (Fig. 2c). This improves the representation of particles larger than 30 μm, reducing the total variation distance metric (Gibbs and Su, 2002, , a 2D analog to the root mean square error) from 0.52 to 0.35. However, the model still strongly underestimates the number densities of small ice crystals, indicating errors in parameterizing ice formation under cirrus conditions.

The second modification addresses the deposition freezing parameterization, which was incorrectly active at temperatures both below and above the homogeneous freezing threshold. Originally calibrated for temperatures warmer than -25°C (Fig. 1), this parameterization extended far beyond its intended range. We restrict it to T>-37°C and introduce a scheme to account for competition between homogeneous and heterogeneous nucleation at T<-37°C (Liu and Penner, 2005; Shi et al., 2015). This scheme captures low ICNC heterogeneous nucleation at RH$_{ice}$ $> 120\%$ while also allowing for homogeneous nucleation events under sufficiently strong updrafts and high RH$_{ice}$.

The two changes cut the microphysical bias in half, improving the representation of both small and large particles (Fig. 2d). Nevertheless, some substantial biases remain. The model continues to underestimate ICNC for small ice crystals and overestimate ICNC for larger crystals that represent freshly detrained particles (Fig. **??**a-b). These remaining biases largely stem from persistent challenges in representing ice microphysics (see Discussion) and from too low vertical wind variance in the model (see Section 4.3).

Cirrus cloud properties in tropical aircraft measurements (first column) and SAM model simulations with improved microphysics at 1 km horizontal grid spacing (second column). Lines represent median values. Gray lines in the middle column represent median values of the standard model setup. The third column shows the anomalies between SAM and aircraft data; the lines are copies of the lines on the first and second column panels. The data is sorted into 4°C temperature bins. The values in each temperature bin add up to 100%.

To provide an alternative perspective, we examine the model's performance by sorting results by temperature. The exponential decrease in IWC with decreasing temperature, as expected from the Clausius-Clapeyron relationship, has improved compared to the standard model version and is well represented by the model (Fig. **??**a-c). Observed ICNC shows large variability, with more than one order of magnitude increase in the median number between temperatures of -40°C and -70°C (Fig. **??**d). The model reproduces the observed median and spread for temperatures warmer than -65°C but underestimates ICNC at the coldest temperatures, although this bias has been substantially improved compared to the standard model version (only gray median shown). This bias aligns with the underrepresentation of small particles highlighted in Fig. 2. Insights from tracers (Fig. **??**) suggest the bias may stem from too few in situ nucleated particles or insufficient detrainment of small particles from deep convection.

Similarly to IWC, the mean mass radius decreases with temperature, with medians ranging from 80 μm at -40°C to 15 μm at -80°C. The model simulates particles that are too small at warmer temperatures (between -55°C and -40°C) and slightly too

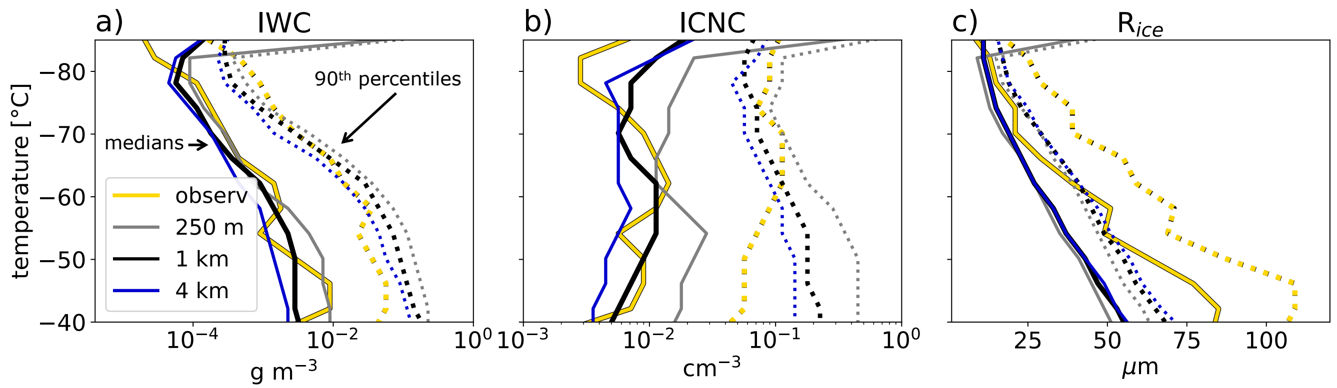

Figure 8. Grid spacing dependence of (a) ice water content (IWC), (b) ice crystal number concentration (ICNC), and (c) ice radius (R_{ice}) in SAM with improved microphysics compared to aircraft observations (in yellow). All data are regridded to a horizontal resolution of 4 km. Plotted are median values (solid lines) and 90th percentile values (dotted lines).

large at T <-70°C. Notably, the spread in simulated particle size is narrower than observed, possibly due to the too simple single-mode description of ice microphysics (see Discussion).

In summary, the temperature-sorted model results offer a complementary perspective on cirrus cloud properties, showing good agreement with observations for temperatures warmer than -60°C while highlighting persistent biases at colder temperatures. Nevertheless, this agreement represents a substantial improvement compared with the earlier model version (Fig. 2), emphasizing processes where further refinement is still needed. The addition of passive tracers discussed in section 3 helps pinpoint processes requiring further refinement, particularly the representation of in situ ice nucleation at cold temperatures.

Horizontal grid spacing dependence

4.4 Impact on cloud properties

All results presented so far are based on simulations with a horizontal grid spacing of 1 km, which is sufficient to represent anvil cloud evolution and their influence on mesoscale circulation (Gasparini et al., 2019, 2022). To assess the impact of model grid spacing, we include additional simulations at coarser (4 km) and finer (250 m) grid spacings. The 4 km grid spacing aligns with current GSRMs, while the 250 m grid spacing approaches the level of convergence for deep convective updraft strength in idealized and realistic tropical convection setups (Khairoutdinov et al., 2009; Jeevanjee et al., 2017) (Khairoutdinov et al., 2009; Jeevanjee, 2017; Prein et al., 2025).

The sensitivity of simulated ice properties to horizontal grid spacing is most pronounced for ICNC, which increases by nearly an order of magnitude from the 4 km to the 250 m simulation, a trend also evident in the 90th percentiles (Fig. ??8b). IWC exhibits grid spacing dependence only at temperatures warmer than -60°C, with higher values at finer grid spacings (Fig. ??8a). In contrast, ice crystal radius shows little sensitivity to grid spacing (Fig. ??8c). Moreover, SAM underestimates the variability in ice crystal size across all grid spacings and fails to reproduce the 90th percentile of observed particle size.

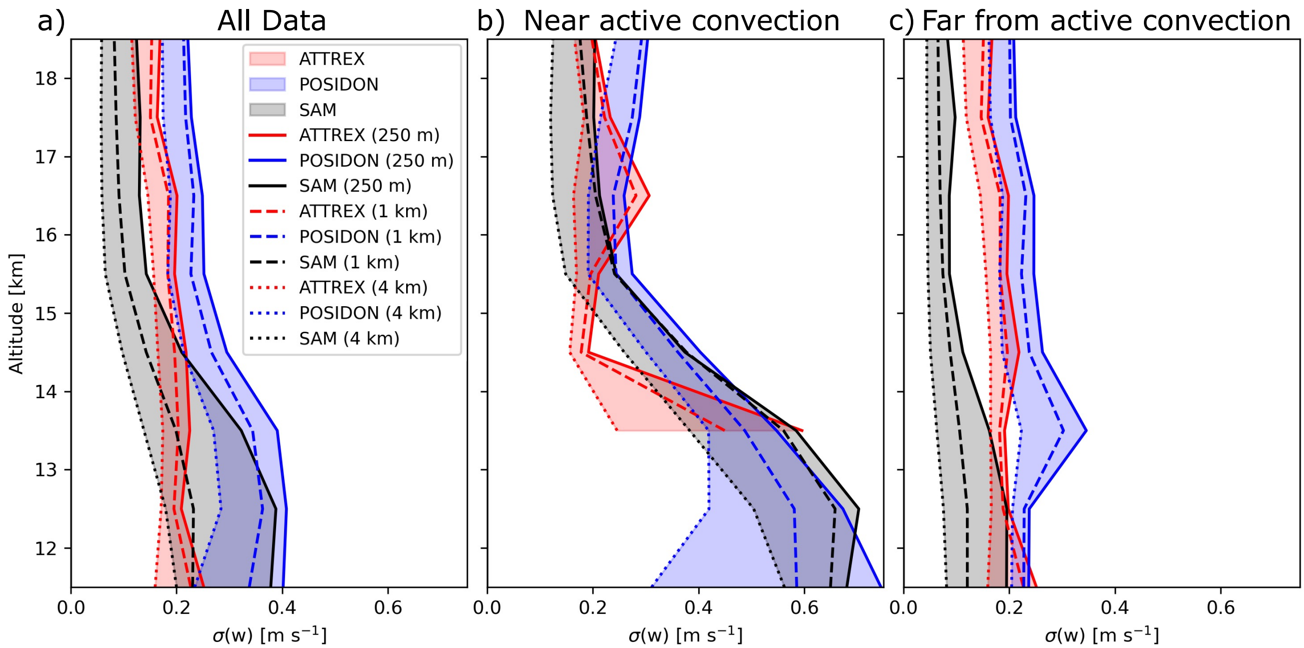

Figure 9. Standard deviation of ~~updrafts~~ vertical wind from simulations with the improved SAM model and aircraft observations for (a) all data, (b) locations near active deep convection (brightness temperatures $<$ 240 K), and (c) areas far from active deep convection (brightness temperatures $>$ 240 K).

Overall, simulated microphysical properties at all grid spacings fall within the range of observations. However, the 4 km simulations underestimate both IWC and ICNC across most temperatures, but these biases are ~~reduced~~ gone in the 1 km simulation. The ice number–radius perspective provides a clearer view of these improvements, particularly for the low ICNC bias of ice crystals smaller than 30 μm (Fig. A1). ~~Increasing grid spacing helps to better~~ Increased model resolution helps identify and understand the sources of model bias. The following section explores ~~updraft~~ vertical wind variability, a likely contributor to these biases and a key factor in the reduced model bias observed for finer horizontal grid spacing.

4.5 Vertical wind variability

Ice formation is strongly influenced by the availability of water vapor and on the supersaturation with respect to ice, which depends on the dynamical environment. ~~Accurately capturing updraft variability is thus critical for modeling cirrus cloud formation and properties (Barahona et al., 2017).~~ Of particular significance are the high-frequency fluctuations, which are approximately ten times larger than the slow synoptic scale motions (Atlas and Bretherton, 2023). Accurately capturing vertical wind variability is thus critical for modeling cirrus cloud formation and properties (Barahona et al., 2017).

The biases in ~~microphysical properties, especially ICNC ,~~ extreme ICNC values align with the model's underestimate of strong updrafts. This results in a too narrow ~~updraft~~ vertical wind distribution and an underestimated standard deviation (Fig.

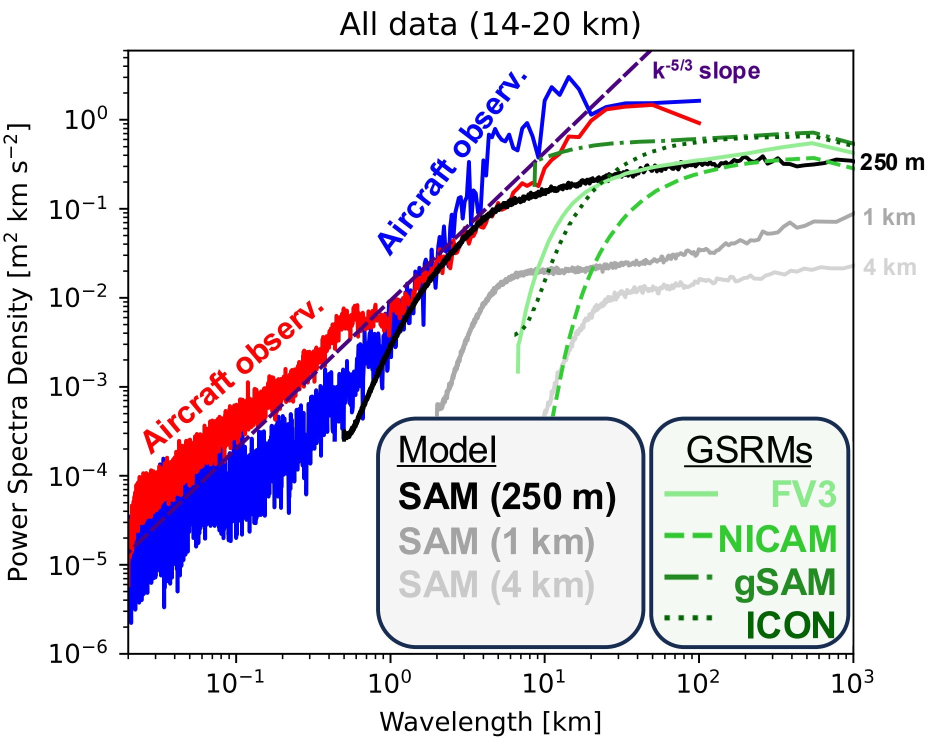

Figure 10. Power spectrum of updrafts from ATTREX (red) and POSIDON (blue) aircraft measurements, improved SAM model simulations (in grayscale), and a selection of GSRMs (in green). The dashed pink line represents the $k^{-5/3}$ slope, where k is the wavenumber.

??9). Including a subgrid-scale updraft velocity term minimally vertical wind term (Sec. 2.1.5) slightly improves the issue slightly by increasing the standard deviation in updrafts vertical wind by 1-10% depending on the model grid spacing (2-4% for 1 km grid spacing). Nevertheless, the model performs well in representing the updraft vertical wind variability near regions of deep convection at all three horizontal grid spacings (4 km, 1 km, 250 m) (Fig. ??9b).

However, updraft variability is strongly underestimated in regions far from deep convection (defined as areas with brightness temperature $>$ 240 K) for simulations at 4 and 1 km grid spacing. The 250 m simulation shows better agreement with the measured winds below 14 km, where anvil cloud coverage is the largest, but underestimates wind variability in the TTL, resultign resulting in a persistent ICNC bias for small ice crystals (Fig A1c and f). This also likely contributes to larger microphysical biases in clouds far from active convection compared to those near convection (Fig. A2).

Power spectra in Fig. ??10, calculated following Atlas and Bretherton (2023), provide further insight into updraft variability accross across different wavelengths of atmospheric disturbances. Variability at wavelengths larger than $\sim$1000 km corresponds to synoptic-scale motion, while convectively generated gravity waves dominate at wavelengths between 1 and 1000 km. Turbulent processes of various sources dominate at wavelengths below $\sim$200 m.

As already shown by Fig. ??9, wind variance increases with finer horizontal grid spacing. While the 4 and 1 km simulations substantially underestimate wind variance and power, the 250 m simulation reproduces the observed wind variability for wavelengths between 1 and 10 km. Moreover, all SAM simulations under-represent variability at scales larger than ∼100 km, which are better captured by GSRMs at horizontal grid spacings of about 4 km. Vertical wind spectra from models flatten out at the model effective resolution, which varies across the different GSRMs and SAM simulations shown in Figure 10. Aircraft observations are most suitable for investigating vertical wind variability $<$ 10 km and flatten out between 10 and 100 km possibly due to a smaller signal-to-noise ratio, limited data, and/or changing atmospheric dynamics. Gravity waves, originating from deep convective updrafts, propagate hundreds to thousands of kilometers from their source. However, the narrow channel setup of the SAM simulation restricts the generation may restrict the generation and/or propagation of these waves compared to the real atmosphere or global GSRM simulations. While larger-scale updraft variability fosters favorable conditions for deep convection, its direct contribution to cloud formation is limited and of secondary importance for this study.

4.6 The relevance of tropical cirrus for top-of-the-atmosphere radiative fluxes

(a) Frequency of cloud occurrence in each ice water path (IWP) bin, (b) average CRE in each IWP bin, and (c) the contribution of each IWP bin to the CRE. The gray shading in panel a) highlights the range of observations. Panels b) and c) show results only for the improved SAM model and the CCCM satellite product. Model results are presented in its full resolution, and regridded to 36×36 km grid, similar to the resolution of CERES satellite retrievals of CRE.

To link cirrus cloud properties to the TOA radiative budget, we take an integrated perspective and categorize cloud occurrence frequency and radiative effects based on IWP. Figure **??**a compares the simulated IWP distribution with four satellite-derived datasets, showing that the improved model generally falls within or near the observed range. The apparent overrepresentation of the thinnest cirrus in the model and the corresponding slight underestimation of other cloud types in the normalized PDF should not be interpreted as a bias, as satellite retrievals are known to underestimate the thinnest cirrus clouds (Balmes and Fu, 2018; Lesigne et al., . We also find that thin cirrus with IWP $<$ 1 g m^{-2} constitute 52% of all simulated cirrus but contribute only 6% to the LW CRE and 5% to the SW CRE. This suggests that while thin cirrus are frequent, their direct radiative impact at the TOA is limited. Restricting the analysis to the most radiatively important clouds with IWP $>$ 1 g m^{-2} improves the model agreement with satellite observations (Fig. B1).

Figure **??**b shows the averaged CRE for high clouds in each IWP bin. The most frequent anvils according to satellite datasets occur at an IWP of 3-30 g m^{-2}, which corresponds to anvil clouds of intermediate optical depth (1-3) that yield a net positive, LW-dominated CRE (Sokol and Hartmann, 2020). For thicker clouds (IWP $>$ 100 g m^{-2}), both model and satellite data show a dominance of SW CRE, with net CRE exceeding -100 W m^{-2} for the thickest anvils. However, the model overestimates the SW CRE, a bias partially resolved by averaging the output onto coarser grid scales, similar to the CERES pixel data resolution (36×36 km grid boxes). Additionally, a recently identified bug in the ice optics parameterization likely increased the optical depth and radiative effects per unit IWP by ∼15%, but this issue could not be addressed in the current simulations. This SW bias becomes even more apparent when comparing CERES CRE retrieved during daytime satellite overpasses with model-simulated CRE between 1 and 2 pm local time (Fig. B2b).

Determining which type of tropical cirrus is radiatively most important is not straightforward. Are the less frequent but thick deep convective cores and fresh anvils, which have a strong influence on both SW and LW CRE, the most dominant, or do the more widespread anvil clouds of intermediate thickness dominate? Figure **??**c provides an answer by scaling the CRE in a given IWP bin by that bin's frequency of occurrence: the radiatively most dominant clouds have IWP between 30 and 3000 g m^{-2}, similar to results by Berry and Mace (2014). These include anvil clouds with optical depths greater than approximately 1. Nonetheless, thinner cirrus (IWP 1–30 g m^{-2}, Fig. **??**c) also contribute meaningfully to the net CRE, underscoring the importance of studying not only the thickest tropical cirrus but also their continued evolution until they reach an IWP of $\sim$0.1 g m^{-2} (optical depth $\sim$0.1). Additionally, the response of thin cirrus to global warming remains highly uncertain (Sokol et al., 2024), and deserves further investigation.

This analysis, together with our previous findings (Fig. **??**), provides more information about the evolution of tropical cirrus. These can be split into two separate evolution pathways, as depicted in Fig. **??**a. Thick anvils originating in high IWP deep convective towers spread and thin towards IWP $\sim$1 g m^{-2}, while thinner cirrus (IWP $<$ 1 g m^{-2}) predominantly form via in situ ice nucleation. Despite their smaller radiative impact, these thin cirrus are highly frequent and likely play a much larger role in shaping TTL temperatures and influencing deep convective overshoot frequencies (Fu et al., 2018; Hu et al., 2021). Both phases are associated with substantial uncertainties in their microphysical properties and radiative impacts. Addressing these uncertainties is essential for improving our understanding of cirrus feedbacks in the climate system and will be the focus of follow-up studies.

5 Discussion

5.1 Ice microphysics

The representation of ice microphysics remains a limitation in this study, despite notable improvements achieved with the described computationally inexpensive changes. This reflects the broader challenge of accurately modeling ice microphysics in high-resolution models, where computational constraints and incomplete process understanding often impose trade-offs.

For example, the adopted Shi et al. (2015) scheme for ice nucleation, originally designed for coarse climate models, relies on empirical fits to parcel model simulations. While effective, this approach may not capture all the details of ice nucleation at cloud-resolving scales accurately. Future work could address this by implementing a physics-based nucleation scheme, such as the novel Kärcher (2022) scheme . Moreover, a bug was discovered in processing of in situ observations after we had completed the simulations and this prevented us to resolve the model's issue of underestimating small particles with high ice crystal number concentrations. While model tuning could partially resolve this issue, a more robust solution would involve implementing a more realistic nucleation scheme and /or incorporating and incorporate a resolution-aware parameterization of wind variability to complement the model-resolved wind variability – similar to approaches being developed for liquid clouds (Salesky et al., 2024).

Secondary ice formation may be another area of interest, given that recent studies have shown that it plays a large role even at temperatures as cold as -50°C (Hawker et al., 2021; Huang et al., 2022; Qu et al., 2022). Incorporating secondary ice pro-

cesses into SAM-P3 currently requires additional computationally expensive ice modes, but their inclusion could enhance the model's ability to simulate anvil cloud evolution. Finally, increased model complexity brings additional challenges, often resulting in hindered process understanding, increased uncertainty, or the problem of equifinality (refer to Proske et al. (2023) and references therein for a complete outline of these issues)(refer to Proske et al., 2023, and references therein for a complete outline of these i
.

An alternative approach could involve introducing ice tracers for each ice nucleation process, similar to those used by Lüttmer et al. (2024). This would allow for a more accurate classification of cirrus cloud origins without relying on arbitrary thresholds. Although this would modestly increase the model's computational costs, the expense is substantially lower than doubling the model's resolution, making it a viable path forward.

5.2 Resolution and Lagrangian approaches

Our findings confirm that increasing horizontal resolution improves the representation of atmospheric updrafts at scales crucial for cirrus cloud formation. However, this improvement comes at a large cost: a 4-fold increase in horizontal resolution results in a 16-fold increase in data output and a 25-30-fold 20-25-fold increase in computational demand. This highlights the importance of exploring less computationally expensive alternatives to improve model performance. For instance, we achieved a large reduction in bias for ice cloud properties through straightforward modifications to the ice microphysics without appreciable increases in computational cost.

Encouragingly, the simulations at a typical GSRM grid spacing of 3-5 km show signs of convergence in updraft variability near active deep convection when compared to updraft observations averaged to same grid spacing, suggesting that the generation of convective gravity waves is reasonably well captured (note that model-simulated updraft variability still increases between simulations of 4 and 1 km grid spacing). However, these waves do may not propagate far enough, as indicated by the underestimated updraft variance across all tested horizontal resolutions. Power spectral analyses indicate that grid spacings slightly finer than 250 m may sufficiently capture the scales of motion relevant for cirrus formation and maintenance. This is also the grid spacing at which convergence in cloud macroscopic variables and ice sources and sinks has been observed (Hu et al., 2024).

Vertical resolution also plays a crucial role. Previous studies demonstrate its influence on tropical cirrus properties , and their responses to global warming (Ohno et al., 2019), and convective self-aggregation (Jenney et al., 2023). We also perform a short sensitivity test that doubles halves the vertical grid spacing from 200 m to 100 mincreased updraft variability away from deep convection while raising , leading to the same model improvement as an increase in horizontal grid spacing from 1 km to 250 m (Fig. A1g). Doubling the vertical resolution in the upper troposphere increases the computational costs by only a factor of 4.5 (not shown). 2.5. This suggests that refining vertical resolution could be a more computationally efficient way to improve model updraft variability than increases in horizontal resolution, and it should be thoroughly investigated in future studies.

Nevertheless, higher resolution alone cannot address all challenges. Processes at microscopic scales, particularly the interactions between ice microphysics and radiation, remain poorly resolved. Efforts to improve ice microphysics in GSRMs are scarce (e.g., Seiki and Ohno, 2022), yet essential for advancing understanding of tropical cirrus evolution. Our study highlights the importance of accurately modeling cirrus evolution, a key factor in determining their microphysical properties and radiative effects.

Passive tracers, as demonstrated in this study, are a valuable tool for tracking the evolution of ice clouds in models. Although these tracers are purely computational, stable water isotopes, measurable in situ or via satellite, could serve as real-world tracer analogs, offering insights into the pathways of ice cloud evolution (Blossey et al., 2010; de Vries et al., 2022). Trajectory analysis, such as that in Sullivan et al. (2022), can provide additional clarity on cirrus cloud evolution. Based on their analysis of cloud source and sink processes along trajectories, they proposed three cirrus cloud lifecycles with distinct radiative signatures. In contrast, our analysis focused only on ice cloud properties. However, by enabling the 3D output of microphysical process rates, we could easily perform a similar process-rate analysis that would provide additional clarity on the two tropical cirrus formation pathways. Future work could explore a consistent integration of these approaches in models and observations, linking simulations with aircraft measurements as in Froyd et al. (2022) and possibly satellite retrievals as well, in an effort to improve process understanding.

6 Conclusions

The purpose of this work is twofold: first, we demonstrate the usefulness of passive tracers to track the evolution of cirrus microphysical properties. Second, we show that minor changes to cloud microphysics that substantially improve the simulation of tropical cirrus at cloud-resolving scales with a minimal change in computational expense.

Our work reveals a simple, numerically inexpensive recipe that substantially improves simulations of tropical cirrus in the SAM cloud-resolving model. Although the recipe was tested only in this specific model, we believe that its elements can be applied to a wider range of models with little or no increase in computational load. The recipe is as follows:

1. Remove all non-physical microphysical limits (particularly the commonly used ICNC limits, see e.g. Bacer et al., 2021).

2. Ensure that freezing (or any other) parameterizations do not operate outside of their stated range of validity (e.g. limit mixed-phase freezing parameterizations to mixed-phase conditions).

3. If not present, add a nucleation scheme that is active under cirrus conditions, e.g. homogeneous nucleation of water solution droplets or a combination of homogeneous and heterogeneous nucleation.

We show that anvil clouds remain radiatively important hours after detrainment, ~~after having undergone~~ despite substantial spreading, thinning, and advection by synoptic and/or mesoscale motion. Therefore, an evolutionary perspective on tropical cirrus is crucial for constraining their radiative impacts. ~~The implementation of passive tracers enables an evolutionary perspective on tropical cirrus clouds. We~~ To better capture this evolution, we implemented two passive tracers ~~to track the three-dimensional evolution of cloud parcels through two distinct perspectives, namely~~in the model:

1. A detrainment ~~perspective~~tracer, useful for tracking the evolution of anvil clouds.

2. An ice nucleation ~~perspective~~tracer, useful for tracking the evolution of in situ cirrus.

Tracers also provide important insights into the climatology of cirrus cloud formation. We find that in situ cirrus dominate under colder conditions ($\geq$70% of cirrus at temperatures below -70°C) and are prevalent at low ice water path values (IWP< 1 g m^{-2}). Despite their low optical depth, ~~these clouds cannot be neglected in the TOA radiative balance analysis~~in situ cirrus account for 7% of the total tropical cirrus TOA CRE. However, our estimates are sensitive to the specific classification criteria used for cloud origin and lacks considerations of cloud overlap, highlighting the need for more refined approaches. ~~A more accurate, but also computationally more expensive model setup with multiple ice species will address this uncertainty in a follow-up study.~~

Our results also suggest that simulations with horizontal grid spacing of 250 m can reproduce the observed power spectrum of vertical wind, capturing the scales of motion relevant for cirrus formation and maintenance, particularly below 14 km.

More broadly, our work highlights a significant limitation in existing global climate and cloud-resolving models, many of which fail to accurately simulate tropical cirrus evolution (Wall and Hartmann, 2018; Turbeville et al., 2022; Atlas et al., 2024). These biases ~~prevent the understanding of~~ pose difficulties for understanding the processes that occur between the formation of tropical cirrus and their dissipation (Gasparini et al., 2023), leaving large uncertainties in the associated climate feedbacks (Sherwood et al., 2020). Additionally, the interaction of ice crystals with radiation, which influences atmospheric temperatures, can alter cloud lifetimes (Gasparini et al., 2022), regional climate (Voigt et al., 2019), and hydrological sensitivity (McGraw et al., 2025), with potentially important impacts as high clouds shift upward in a warming climate (Voigt et al., 2024; Gasparini et al., 2024). By addressing these gaps, we have demonstrated that our improved SAM model is now equipped to explore these feedbacks with greater confidence.

Building on the advancements presented here, future studies should focus on reducing uncertainties in the fundamental understanding and modeling of cirrus properties and their evolution in the present and in a warmer climate. The combination of passive tracers, improved microphysics, and high-resolution modeling provides a promising pathway to ~~achieving~~ achieve this goal.

Video supplement. A video supplement showing the evolution of clouds in part of the model domain between days 22.75 and 27.75 is available at https://doi.org/10.5281/zenodo.15497521. The panels visualize quantities shown in Figure 5.

Appendix A: Additional model evaluation

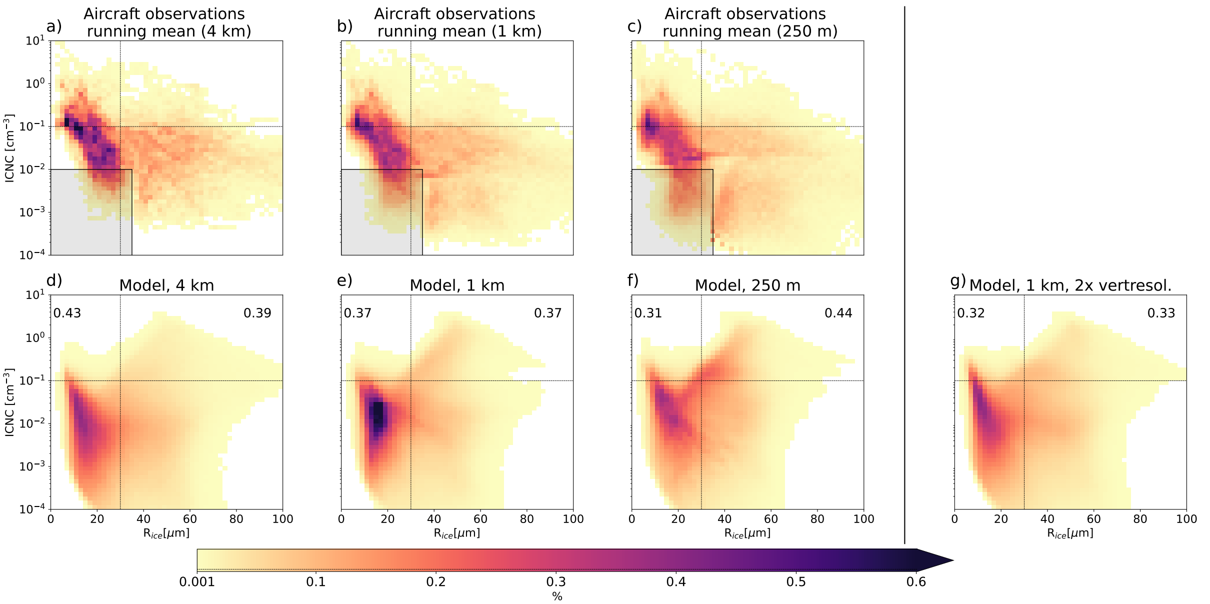

Figure A1. Model grid spacing dependence in the ICNC-R_{ice} space. Probability density function of ice properties for clouds at T<-40°C. The upper row shows aircraft observations averaged for consistency to 4 km, 1 km, and 250 m grid. Panels d-f show modeled properties at different horizontal ~~resolutions~~grid spacings. Panel g) shows modeled properties at 1 km horizontal grid spacing and doubled upper tropospheric vertical grid spacing (to about 100 m). The number represents a two-dimensional total variation distance of model data compared to aircraft observations (the smaller, the better). Observations are limited or not available in the shaded area.

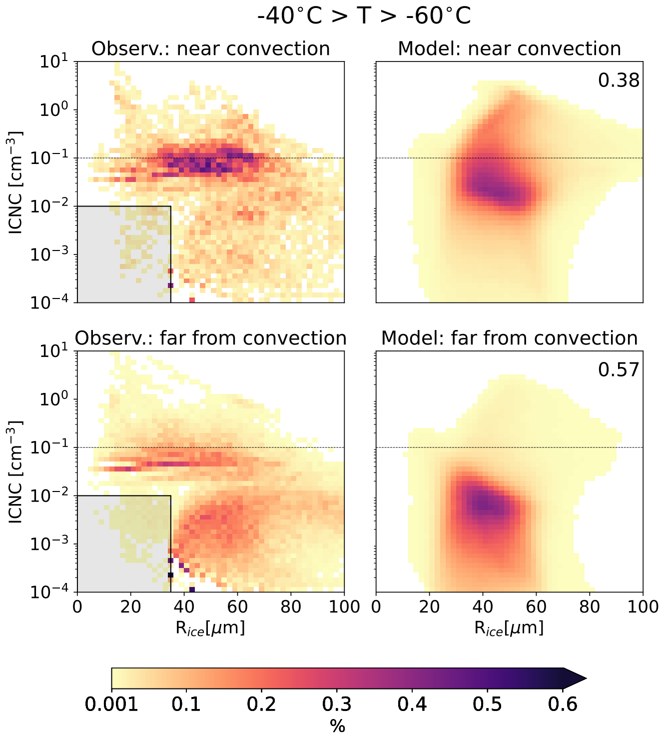

Figure A2. Probability density function of ice properties near (brightness temperature < 240 K) and far from active convection (brightness temperature > 240 K) at -40°C> T >-60°C. The number on the right is the dimensional total variation distance of model data compared to aircraft observations (the smaller, the better). Observations are limited or not available in the shaded area.

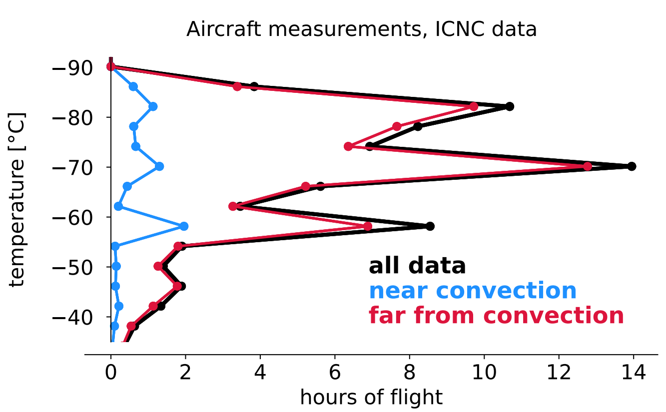

Figure A3. Number of measurement hours for ICNC data. The measurement frequency is 1 Hz, so 1 hour corresponds to 3600 measurements. The R_{ice} data have the same number of flight hours, while there are slightly more IWC data.

Appendix B: Additional IWP-binned perspective on model output and satellite observations

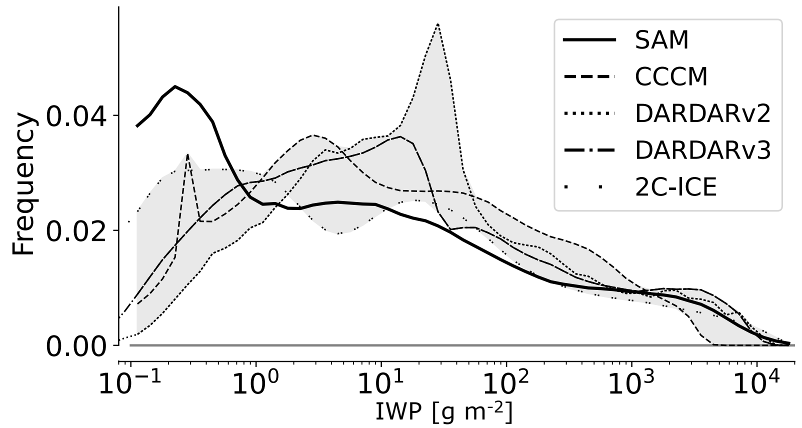

Figure B1. Ice water path (IWP) binned occurrence frequency. As in Fig. ??4a, but for IWP>0.1 g m^{-2}.

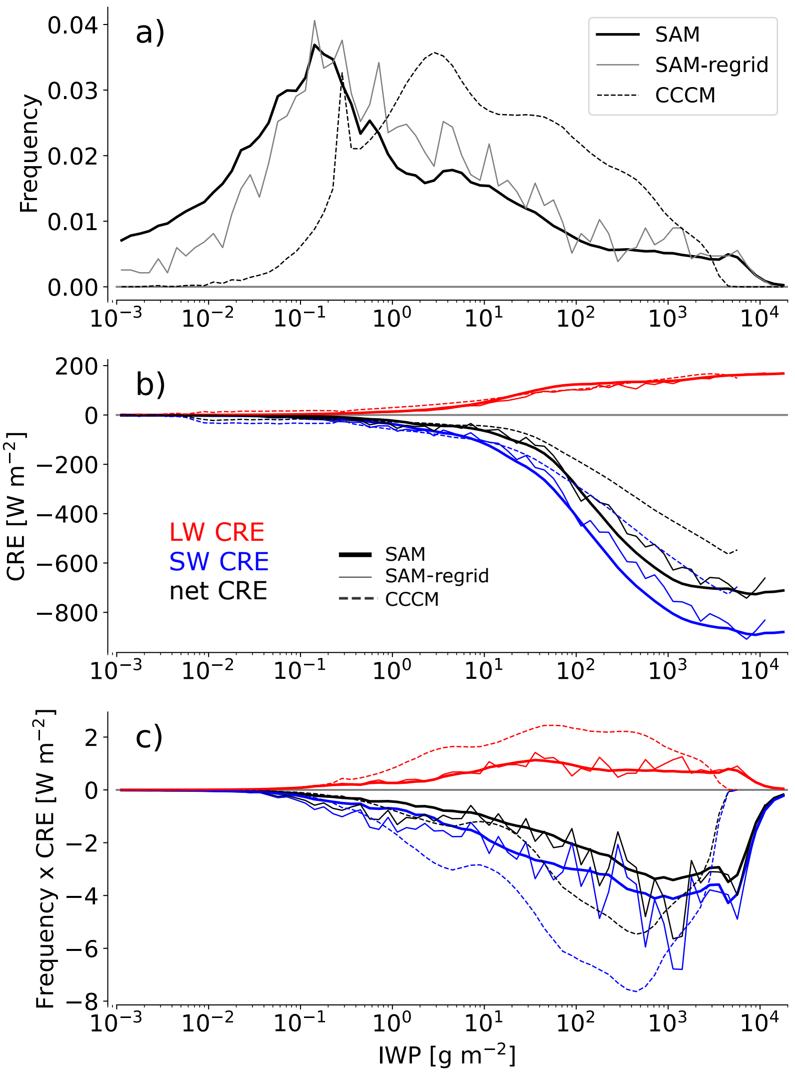

Figure B2. Daytime-only ice water path (IWP) binned cloud occurrence and radiative effect. The figure is similar to Fig. ??4, but with (1) model results for 1 and 2 pm local time only and (2) CCCM SW radiative fluxes computed as a difference between clear and full sky radiation.

Code and data availability. Data, plotting and post-processing scripts, key (modified) bits of the SAM model Fortran code are available on Zenodo at https://doi.org/10.5281/zenodo.14674413. The complete SAM model code is available for download at https://you.stonybrook.edu/somas/sam/. Satellite data from the A-Train Integrated CALIPSO, CloudSat, CERES, and MODIS Merged Product Release B1 (CCCM) were obtained from https://search.earthdata.nasa.gov. The DARDAR data are available at http://www.icare.univ-lille1.fr/. The 2C-ICE data are available at https://www.cloudsat.cira.colostate.edu. The POSIDON, ATTREX, and CONTRAST data used in this study are available at https://b2share.fz-juelich.de/records/266ca2a41f4946ff97d874bfa458254c.The original campaign data can be retrieved at https://espoarchive.nasa.gov/archive/browse/posidon/WB57 (POSIDON), https://espo.nasa.gov/attrex/content/Welcome_to_the_ESPO_Data_Archive (ATTREX), and https://www2.acom.ucar.edu/contrast (CONTRAST).

Author contributions. B.G.: conceived the study, implemented code changes, conducted model simulations, processed the majority of the data, and contributed to writing and editing; R.A.: processed part of the data and contributed to writing and editing; A.V.: contributed to writing and editing; M.K.: acquired and processed data, and contributed to writing and editing; P.N.B.: implemented code changes, provided technical support, and contributed to writing and editing.

Competing interests. One of the co-authors is a member of the editorial board of *Atmospheric Chemistry and Physics*. The authors have no other competing interests to declare.

Acknowledgements. BG and AV acknowledge funding received from the European Union's Horizon 2020 research and innovation programme under the Marie Skłodowska-Curie grant agreement No 101025473. RA acknowledges funding received from the European Union's Horizon 2020 research and innovation programme under the Marie Skłodowska-Curie grant agreement No 101151941. This material is based upon work supported by the National Science Foundation under Grant No. OISE-1743753 (PB). We would also like to acknowledge high-performance computing support from Cheyenne (https://doi.org/10.5065/D6RX99HX) and Derecho (https://doi.org/10.5065/qx9a-pg09) provided by NCAR's Computational and Information Systems Laboratory, sponsored by the National Science Foundation. The authors would like to thank Bernd Kärcher for useful comments on early work leading to this manuscript. We acknowledge the use of several AI tools to improve the language and clarity of this manuscript. We thank the reviewers for their constructive comments that improved the manuscript.

References

Achatz, U., Alexander, M. J., Becker, E., Chun, H.-Y., Dörnbrack, A., Holt, L., Plougonven, R., Polichtchouk, I., Sato, K., Sheshadri, A., Stephan, C. C., van Niekerk, A., and Wright, C. J.: Atmospheric Gravity Waves: Processes and Parameterization, Journal of the Atmospheric Sciences, 81, 237–262, https://doi.org/10.1175/JAS-D-23-0210.1, 2024.

Ansmann, A., Tesche, M., Althausen, D., Müller, D., Seifert, P., Freudenthaler, V., Heese, B., Wiegner, M., Pisani, G., Knippertz, P., and Dubovik, O.: Influence of Saharan Dust on Cloud Glaciation in Southern Morocco during the Saharan Mineral Dust Experiment, Journal of Geophysical Research Atmospheres, 113, 1–16, https://doi.org/10.1029/2007JD008785, 2008.

Atlas, R. and Bretherton, C. S.: Aircraft Observations of Gravity Wave Activity and Turbulence in the Tropical Tropopause Layer: Prevalence, Influence on Cirrus Clouds, and Comparison with Global Storm-Resolving Models, Atmospheric Chemistry and Physics, 23, 4009–4030, https://doi.org/10.5194/acp-23-4009-2023, 2023.

Atlas, R., Bretherton, C. S., Sokol, A. B., Blossey, P. N., and Khairoutdinov, M. F.: Tropical Cirrus Are Highly Sensitive to Ice Microphysics Within a Nudged Global Storm-Resolving Model, Geophysical Research Letters, 51, e2023GL105 868, https://doi.org/10.1029/2023GL105868, 2024.

Avery, M., Winker, D., Heymsfield, A., Vaughan, M., Young, S., Hu, Y., and Trepte, C.: Cloud Ice Water Content Retrieved from the CALIOP Space-Based Lidar, Geophysical Research Letters, 39, 2–7, https://doi.org/10.1029/2011GL050545, 2012.

Bacer, S., Sullivan, S. C., Sourdeval, O., Tost, H., Lelieveld, J., and Pozzer, A.: Cold Cloud Microphysical Process Rates in a Global Chemistry-Climate Model, Atmospheric Chemistry and Physics, 21, 1485–1505, https://doi.org/10.5194/acp-21-1485-2021, 2021.

Balmes, K. A. and Fu, Q.: An Investigation of Optically Very Thin Ice Clouds from Ground-Based ARM Raman Lidars, Atmosphere, 9, https://doi.org/10.3390/atmos9110445, 2018.

Barahona, D., Molod, A., and Kalesse, H.: Direct Estimation of the Global Distribution of Vertical Velocity within Cirrus Clouds, Scientific Reports, 7, 6840, https://doi.org/10.1038/s41598-017-07038-6, 2017.

Barklie, R. H. D. and Gokhale, N. R.: The Freezing of Supercooled Water Drops. Alberta Hail,, McGill University Stormy Weather Group Science Rep., MW-30, 43–65, https://doi.org/B, 1959.

Berry, E. and Mace, G. G.: Cloud Properties and Radiative Effects of the Asian Summer Monsoon Derived from A-Train Data, Journal of Geophysical Research Atmospheres, 119, 9492–9508, https://doi.org/10.1002/2014JD021458, 2014.

Bigg, E. K.: The Supercooling of Water, Proceedings of the Physical Society. Section B, 66, 688, https://doi.org/10.1088/0370-1301/66/8/309, 1953.

Blossey, P. N., Kuang, Z., and Romps, D. M.: Isotopic Composition of Water in the Tropical Tropopause Layer in Cloud-Resolving Simulations of an Idealized Tropical Circulation, Journal of Geophysical Research Atmospheres, 115, 1–23, https://doi.org/10.1029/2010JD014554, 2010.

Bramberger, M., Alexander, M. J., Davis, S., Podglajen, A., Hertzog, A., Kalnajs, L., Deshler, T., Goetz, J. D., and Khaykin, S.: First Super-Pressure Balloon-Borne Fine-Vertical-Scale Profiles in the Upper TTL: Impacts of Atmospheric Waves on Cirrus Clouds and the QBO, Geophysical Research Letters, 49, e2021GL097 596, https://doi.org/10.1029/2021GL097596, 2022.

Bretherton, C. S.: Challenges in Numerical Modeling of Tropical Circulations, in: The Global Circulation of the Atmosphere, vol. 3026330, pp. 302–330, 2007.

Bretherton, C. S., Blossey, P. N., and Peters, M. E.: Interpretation of Simple and Cloud-Resolving Simulations of Moist Convection–Radiation Interaction with a Mock-Walker Circulation, Theoretical and Computational Fluid Dynamics, 20, 421–442, https://doi.org/10.1007/s00162-006-0029-7, 2006.

Cazenave, Q., Ceccaldi, M., Delanoë, J., Pelon, J., Groß, S., and Heymsfield, A.: Evolution of DARDAR-CLOUD Ice Cloud Retrievals: New Parameters and Impacts on the Retrieved Microphysical Properties, Atmospheric Measurement Techniques, 12, 2819–2835, https://doi.org/10.5194/amt-12-2819-2019, 2019.

Chang, K.-w. and Ecuyer, T. L.: Influence of Gravity Wave Temperature Anomalies and Their Vertical Gradients on Cirrus Clouds in the Tropical Tropopause Layer – a Satellite-Based View, Atmos. Chem. Phys., 20, 12 499–12 514, https://doi.org/10.5194/acp-20-12499-2020, 2020.

Cooper, W. A.: Ice Initiation in Natural Clouds, Meteorological Monographs, 43, 29–32, https://doi.org/10.1175/0065-9401-21.43.29, 1986.

Corcos, M., Hertzog, A., Plougonven, R., and Podglajen, A.: A Simple Model to Assess the Impact of Gravity Waves on Ice-Crystal Populations in the Tropical Tropopause Layer, Atmospheric Chemistry and Physics, 23, 6923–6939, https://doi.org/10.5194/acp-23-6923-2023, 2023.

Costa, A., Meyer, J., Afchine, A., Luebke, A., Günther, G., Dorsey, J. R., Gallagher, M. W., Ehrlich, A., Wendisch, M., Baumgardner, D., Wex, H., and Krämer, M.: Classification of Arctic, Midlatitude and Tropical Clouds in the Mixed-Phase Temperature Regime, Atmospheric Chemistry and Physics, 17, 12 219–12 238, https://doi.org/10.5194/acp-17-12219-2017, 2017.

de Vries, A. J., Aemisegger, F., Pfahl, S., and Wernli, H.: Stable Water Isotope Signals in Tropical Ice Clouds in the West African Monsoon Simulated with a Regional Convection-Permitting Model, Atmospheric Chemistry and Physics, 22, 8863–8895, https://doi.org/10.5194/acp-22-8863-2022, 2022.

Delanoë, J. and Hogan, R. J.: Combined CloudSat-CALIPSO-MODIS Retrievals of the Properties of Ice Clouds, Journal of Geophysical Research, 115, 1–17, https://doi.org/10.1029/2009JD012346, 2010.

Delanoë, J. M. and Hogan, R. J.: A Variational Scheme for Retrieving Ice Cloud Properties from Combined Radar, Lidar, and Infrared Radiometer, Journal of Geophysical Research Atmospheres, 113, 1–21, https://doi.org/10.1029/2007JD009000, 2008.

DeMott, P. J., Prenni, A. J., Liu, X., Kreidenweis, S. M., Petters, M. D., Twohy, C. H., Richardson, M. S., Eidhammer, T., and Rogers, D. C.: Predicting Global Atmospheric Ice Nuclei Distributions and Their Impacts on Climate, Proceedings of the National Academy of Sciences of the United States of America, 107, 11 217–11 222, https://doi.org/10.1073/pnas.0910818107, 2010.

Deng, M., Mace, Gerald. G., Wang, Z., and Berry, E.: CloudSat 2C-ICE Product Update with a New Ze Parameterization in Lidar-Only Region, Journal of Geophysical Research: Atmospheres, 120, 12,198–12,208, https://doi.org/10.1002/2015JD023600, 2015.

Deng, M., Mace, Gerald. G., and Wang, Z.: Anvil Productivities of Tropical Deep Convective Clusters and Their Regional Differences, Journal of the Atmospheric Sciences, 73, 3467–3487, https://doi.org/10.1175/JAS-D-15-0239.1, 2016.

Deutloff, J., Buehler, S. A., Brath, M., and Naumann, A. K.: Insights on Tropical High-Cloud Radiative Effect From a New Conceptual Model, Journal of Advances in Modeling Earth Systems, 17, e2024MS004 615, https://doi.org/10.1029/2024MS004615, 2025.

Dinh, T., Gasparini, B., and Bellon, G.: Clouds and Radiatively Induced Circulations, in: Cloud Physics and Dynamics: Showers and Shade from Earth's Atmosphere, edited by Sullivan, S. C. and Hoose, C., Geophysical Monograph, pp. 239–253, American Geophysical Union Monograph Series, ISBN 978-1-119-70031-9, 2023.

Flatau, P. J., Walko, R. L., and Cotton, W.: Polynomial Fits to Saturation Vapor Pressure., Journal of Applied Meteorology, 31, 1507–1513, 1992.

Froyd, K. D., Yu, P., Schill, G. P., Brock, C. A., Kupc, A., Williamson, C. J., Jensen, E. J., Ray, E., Rosenlof, K. H., Bian, H., Darmenov, A. S., Colarco, P. R., Diskin, G. S., Bui, T. P., and Murphy, D. M.: Dominant Role of Mineral Dust in Cirrus Cloud Formation Revealed by Global-Scale Measurements, Nature Geoscience, 15, 177–183, https://doi.org/10.1038/s41561-022-00901-w, 2022.

Fu, Q., Smith, M., and Yang, Q.: The Impact of Cloud Radiative Effects on the Tropical Tropopause Layer Temperatures, Atmosphere, 9, 1–13, https://doi.org/10.3390/atmos9100377, 2018.

Gasparini, B. and Lohmann, U.: Why Cirrus Cloud Seeding Cannot Substantially Cool the Planet, Journal of Geophysical Research: Atmospheres, 121, 4877–4893, https://doi.org/10.1002/2015JD024666, 2016.

Gasparini, B., Meyer, A., Neubauer, D., Münch, S., and Lohmann, U.: Cirrus Cloud Properties as Seen by the CALIPSO Satellite and ECHAM-HAM Global Climate Model, Journal of Climate, 31, 1983–2003, https://doi.org/10.1175/JCLI-D-16-0608.1, 2018.

Gasparini, B., Blossey, P. N., Hartmann, D. L., Lin, G., and Fan, J.: What Drives the Life Cycle of Tropical Anvil Clouds?, Journal of Advances in Modeling Earth Systems, 11, 2586–2605, https://doi.org/10.1029/2019MS001736, 2019.

Gasparini, B., Rasch, P. J., Hartmann, D. L., Wall, C. J., and Dütsch, M.: A Lagrangian Perspective on Tropical Anvil Cloud Lifecycle in Present and Future Climate, Journal of Geophysical Research: Atmospheres, 126, 1–26, https://doi.org/10.1029/2020jd033487, 2021.

Gasparini, B., Sokol, A. B., Wall, C. J., Hartmann, D. L., and Blossey, P. N.: Diurnal Differences in Tropical Maritime Anvil Cloud Evolution, Journal of Climate, 35, 1655–1677, https://doi.org/10.1175/jcli-d-21-0211.1, 2022.

Gasparini, B., Sullivan, S. C., Sokol, A. B., Kärcher, B., Jensen, E., and Hartmann, D. L.: Opinion: Tropical Cirrus – from Micro-Scale Processes to Climate-Scale Impacts, Atmospheric Chemistry and Physics, 23, 15 413–15 444, https://doi.org/10.5194/acp-23-15413-2023, 2023.

Gasparini, B., Mandorli, G., Stubenrauch, C., and Voigt, A.: Basic Physics Predicts Stronger High Cloud Radiative Heating With Warming, Geophysical Research Letters, 51, e2024GL111 228, https://doi.org/10.1029/2024GL111228, 2024.

Gibbs, A. L. and Su, F. E.: On Choosing and Bounding Probability Metrics, International Statistical Review, 70, 419–435, https://doi.org/10.1111/j.1751-5823.2002.tb00178.x, 2002.

Hartmann, D. L. and Berry, S. E.: The Balanced Radiative Effect of Tropical Anvil Clouds, Journal of Geophysical Research : Atmospheres, 122, https://doi.org/10.1002/2017JD026460, 2017.

Hartmann, D. L., Gasparini, B., Berry, S. E., and Blossey, P. N.: The Life Cycle and Net Radiative Effect of Tropical Anvil Clouds, Journal of Advances in Modeling Earth Systems, 10, 3012–3029, https://doi.org/10.1029/2018MS001484, 2018.

Hawker, R., Miltenberger, A., Johnson, J., Wilkinson, J., Hill, A., Shipway, B., Field, P., Murray, B., and Carslaw, K.: Model Emulation to Understand the Joint Effects of Ice-Nucleating Particles and Secondary Ice Production on Deep Convective Anvil Cirrus, Atmospheric Chemistry and Physics, 21, 17 315–17 343, https://doi.org/10.5194/acp-21-17315-2021, 2021.

Herbert, R. J., Murray, B. J., Dobbie, S. J., and Koop, T.: Sensitivity of Liquid Clouds to Homogenous Freezing Parameterizations, Geophysical Research Letters, 42, 1599–1605, https://doi.org/10.1002/2014GL062729, 2015.

Hoose, C., Lohmann, U., Erdin, R., and Tegen, I.: The Global Influence of Dust Mineralogical Composition on Heterogeneous Ice Nucleation in Mixed-Phase Clouds, Environmental Research Letters, 3, 025 003, https://doi.org/10.1088/1748-9326/3/2/025003, 2008.

Horner, G. and Gryspeerdt, E.: The Evolution of Deep Convective Systems and Their Associated Cirrus Outflows, Atmospheric Chemistry and Physics, 23, 14 239–14 253, https://doi.org/10.5194/acp-23-14239-2023, 2023.

Hoyle, C. R., Luo, B. P., and Peter, T.: The Origin of High Ice Crystal Number Densities in Cirrus Clouds, Journal of the Atmospheric Sciences, 62, 2568–2579, https://doi.org/10.1175/JAS3487.1, 2005.

Hu, Y., McFarquhar, G. M., Wu, W., Huang, Y., Schwarzenboeck, A., Protat, A., Korolev, A., Rauber, R. M., and Wang, H.: Dependence of Ice Microphysical Properties on Environmental Parameters: Results from HAIC-HIWC Cayenne Field Campaign, Journal of the Atmospheric Sciences, 78, 2957–2981, https://doi.org/10.1175/JAS-D-21-0015.1, 2021.

Hu, Z., Jeevanjee, N., and Kuang, Z.: A Refined Zero-Buoyancy Plume Model for Large-Scale Atmospheric Profiles and Anvil Clouds in Radiative-Convective Equilibrium, Journal of Advances in Modeling Earth Systems, 16, e2023MS004 050, https://doi.org/10.1029/2023MS004050, 2024.

Huang, Q. and Dinh, T.: Tropical Cirrus Clouds of Convective and Non-Convective Origins, Atmospheric Chemistry and Physics Discussions, 2022, 1–20, https://doi.org/10.5194/acp-2022-146, 2022.

Huang, Y., Wu, W., McFarquhar, G. M., Xue, M., Morrison, H., Milbrandt, J., Korolev, A. V., Hu, Y., Qu, Z., Wolde, M., Nguyen, C., Schwarzenboeck, A., and Heckman, I.: Microphysical Processes Producing High Ice Water Contents (HIWCs) in Tropical Convective Clouds during the HAIC-HIWC Field Campaign: Dominant Role of Secondary Ice Production, Atmospheric Chemistry and Physics, 22, 2365–2384, https://doi.org/10.5194/acp-22-2365-2022, 2022.

Iacono, M. J., Delamere, J. S., Mlawer, E. J., Shephard, M. W., Clough, S. A., and Collins, W. D.: Radiative Forcing by Long-Lived Greenhouse Gases: Calculations with the AER Radiative Transfer Models, Journal of Geophysical Research Atmospheres, 113, 2–9, https://doi.org/10.1029/2008JD009944, 2008.

Ickes, L., Welti, A., Hoose, C., and Lohmann, U.: Classical Nucleation Theory of Homogeneous Freezing of Water: Thermodynamic and Kinetic Parameters, Phys. Chem. Chem. Phys., 17, 5514–5537, https://doi.org/10.1039/C4CP04184D, 2015.

Jeevanjee, N.: Vertical Velocity in the Gray Zone, Journal of Advances in Modeling Earth Systems, 9, 2304–2316, https://doi.org/10.1002/2017MS001059, 2017.

Jeevanjee, N., Hassanzadeh, P., Hill, S., and Sheshadri, A.: A Perspective on Climate Model Hierarchies, Journal of Advances in Modeling Earth Systems, 9, 1760–1771, https://doi.org/10.1002/2017MS001038, 2017.

Jeggle, K., Czerkawski, M., Serva, F., Saux, B. L., Neubauer, D., and Lohmann, U.: IceCloudNet: 3D Reconstruction of Cloud Ice from Meteosat SEVIRI, https://doi.org/10.48550/arXiv.2410.04135, 2024.

Jenney, A. M., Ferretti, S. L., and Pritchard, M. S.: Vertical Resolution Impacts Explicit Simulation of Deep Convection, Journal of Advances in Modeling Earth Systems, 15, e2022MS003 444, https://doi.org/10.1029/2022MS003444, 2023.

Jensen, E. J., Lawson, P., Baker, B., Pilson, B., Mo, Q., Heymsfield, a. J., Bansemer, A., Bui, T. P., McGill, M., Hlavka, D., Heymsfield, G., Platnick, S., Arnold, G. T., and Tanelli, S.: On the Importance of Small Ice Crystals in Tropical Anvil Cirrus, Atmos. Chem. Phys., 9, 5519–5537, https://doi.org/10.5194/acp-9-5519-2009, 2009.

Jensen, E. J., Diskin, G., Lawson, R. P., Lance, S., Bui, T. P., Hlavka, D., McGill, M., Pfister, L., Toon, O. B., and Gao, R.: Ice Nucleation and Dehydration in the Tropical Tropopause Layer, Proceedings of the National Academy of Sciences, 110, 2041–2046, https://doi.org/10.1073/pnas.1217104110, 2013.

Jensen, E. J., Pfister, L., Jordan, D. E., Bui, T. V., Ueyama, R., Singh, H. B., Thornberry, T., Rollins, A. W., Gao, R.-S., Fahey, D. W., Rosenlof, K. H., Elkins, J. W., Diskin, G. S., DiGangi, J. P., Lawson, R. P., Woods, S., Atlas, E. L., Navarro Rodriguez, M. A., Wofsy, S. C., Pittman, J., Bardeen, C. G., Toon, O. B., Kindel, B. C., Newman, P. A., McGill, M. J., Hlavka, D. L., Lait, L. R., Schoeberl, M. R., Bergman, J. W., Selkirk, H. B., Alexander, M. J., Kim, J.-E., Lim, B. H., Stutz, J., and Pfeilsticker, K.: The NASA Airborne Tropical TRopopause EXperiment (ATTREX): High-Altitude Aircraft Measurements in the Tropical Western Pacific, Bulletin of the American Meteorological Society, 98, 129–143, https://doi.org/10.1175/BAMS-D-14-00263.1, 2017.

Jensen, E. J., Kärcher, B., Ueyama, R., Pfister, L., Bui, T. V., Diskin, G. S., DiGangi, J. P., Woods, S., Lawson, R. P., Froyd, K. D., and Murphy, D. M.: Heterogeneous Ice Nucleation in the Tropical Tropopause Layer, Journal of Geophysical Research: Atmospheres, 123, 12,210–212,227, https://doi.org/10.1029/2018JD028949, 2018.

Jensen, E. J., Kärcher, B., Woods, S., Krämer, M., and Ueyama, R.: The Impact of Gravity Waves on the Evolution of Tropical Anvil Cirrus Microphysical Properties, Journal of Geophysical Research: Atmospheres, 129, e2023JD039 887, https://doi.org/10.1029/2023JD039887, 2024.

Kärcher, B.: A Parameterization of Cirrus Cloud Formation: Revisiting Competing Ice Nucleation, Journal of Geophysical Research: Atmospheres, 127, e2022JD036 907, https://doi.org/10.1029/2022JD036907, 2022.

Kato, S., Rose, F. G., Sun-Mack, S., Miller, W. F., Chen, Y., Rutan, D. A., Stephens, G. L., Loeb, N. G., Minnis, P., Wielicki, B. A., Winker, D. M., Charlock, T. P., Stackhouse, P. W., Xu, K. M., and Collins, W. D.: Improvements of Top-of-Atmosphere and Surface Irradiance Computations with CALIPSO-, CloudSat-, and MODIS-derived Cloud and Aerosol Properties, Journal of Geophysical Research Atmospheres, 116, 1–21, https://doi.org/10.1029/2011JD016050, 2011.

Khairoutdinov, M. F. and Randall, D. A.: Cloud Resolving Modeling of the ARM Summer 1997 IOP : Model Formulation , Results , Uncertainties , and Sensitivities, Journal of the Atmospheric Sciences, 60, 607–625, https://doi.org/10.1175/1520-0469(2003)060<0607:CRMOTA>2.0.CO;2, 2003.

Khairoutdinov, M. F., Krueger, S. K., Moeng, C.-H., Bogenschutz, P. A., and Randall, D. A.: Large-Eddy Simulation of Maritime Deep Tropical Convection, Journal of Advances in Modeling Earth Systems, 1, 13, https://doi.org/10.3894/james.2009.1.15, 2009.

Kim, J.-E., Alexander, M. J., Bui, T. P., Dean-Day, J. M., Lawson, R. P., Woods, S., Hlavka, D., Pfister, L., and Jensen, E. J.: Ubiquitous Influence of Waves on Tropical High Cirrus Clouds, Geophysical Research Letters, 43, 5895–5901, https://doi.org/10.1002/2016GL069293, 2016.

Köhler, L., Green, B., and Stephan, C. C.: Comparing Loon Superpressure Balloon Observations of Gravity Waves in the Tropics With Global Storm-Resolving Models, Journal of Geophysical Research: Atmospheres, 128, e2023JD038 549, https://doi.org/10.1029/2023JD038549, 2023.

Koop, T., Luo, B., Tsias, A., and Peter, T.: Water Activity as the Determinant for Homogeneous Ice Nucleation in Aqueous Solutions, Nature, 406, 611–614, 2000.

Krämer, M., Rolf, C., Luebke, A., Afchine, A., Spelten, N., Costa, A., Zöger, M., Smith, J., Herman, R., Buchholz, B., Ebert, V., Baumgardner, D., Borrmann, S., Klingebiel, M., and Avallone, L.: A Microphysics Guide to Cirrus Clouds – Part 1: Cirrus Types, Atmospheric Chemistry and Physics, 16, 3463–3483, https://doi.org/10.5194/acp-16-3463-2016, 2016.

Krämer, M., Rolf, C., Spelten, N., Afchine, A., Fahey, D., Jensen, E., Khaykin, S., Kuhn, T., Lawson, P., Lykov, A., Pan, L., Riese, M., Rollins, A., Stroh, F., Thornberry, T., Wolf, V., Woods, S., Spichtinger, P., Quaas, J., and Sourdeval, O.: A Microphysics Guide to Cirrus – Part II: Climatologies of Clouds and Humidity from Observations, Atmospheric Chemistry and Physics, 20, 12 569–12 608, https://doi.org/10.5194/acp-20-12569-2020, 2020.

Lesigne, T., Ravetta, F., Podglajen, A., Mariage, V., and Pelon, J.: Extensive Coverage of Ultrathin Tropical Tropopause Layer Cirrus Clouds Revealed by Balloon-Borne Lidar Observations, Atmospheric Chemistry and Physics, 24, 5935–5952, https://doi.org/10.5194/acp-24-5935-2024, 2024.

Liu, X. and Penner, J. E.: Ice Nucleation Parameterization for Global Models, Meteorologische Zeitschrift, 14, 499–514, https://doi.org/10.1127/0941-2948/2005/0059, 2005.

Lohmann, U., Lüond, F., and Mahrt, F.: An Introduction to Clouds: From the Microscale to Climate, Cambridge University Press, ISBN 978-1-107-01822-8, 2016.

Luebke, A. E., Afchine, A., Costa, A., Meyer, J., Rolf, C., and Spelten, N.: The Origin of Midlatitude Ice Clouds and the Resulting Influence on Their Microphysical Properties, Atmos. Chem. Phys., 16, 5793–5809, https://doi.org/10.5194/acpd-15-34243-2015, 2016.

Lüttmer, T., Spichtinger, P., and Seifert, A.: Investigating Ice Formation Pathways Using a Novel Two-Moment Multi-Class Cloud Microphysics Scheme, EGUsphere, pp. 1–36, https://doi.org/10.5194/egusphere-2024-2157, 2024.

McGraw, Z., Polvani, L. M., Gasparini, B., Van de Koot, E. K., and Voigt, A.: The Cloud Radiative Response to Surface Warming Weakens Hydrological Sensitivity, Geophysical Research Letters, 52, e2024GL112 368, https://doi.org/10.1029/2024GL112368, 2025.

Meyers, M. P., Demott, P. J., and Cotton, W. R.: New Primary Ice-Nucleation Parameterizations in an Explicit Cloud Model, Journal of Applied Meteorology, 31, 708–721, https://doi.org/10.1175/1520-0450(1992)031<0708:NPINPI>2.0.CO;2, 1992.

Mlawer, E. J., Taubman, J., Brown, P. D., Iacono, M. J., and Clough, S. A.: Radiative Transfer for Inhomogeneous Atmospheres: RRTM, a Validated Correlated-k Model for the Longwave, Journal of Geophysical Research, 102, 16 663–16 682, https://doi.org/doi:10.1029/97JD00237, 1997.

Morrison, H. and Milbrandt, J. A.: Parameterization of Cloud Microphysics Based on the Prediction of Bulk Ice Particle Properties. Part I: Scheme Description and Idealized Tests, Journal of the Atmospheric Sciences, 72, 287–311, https://doi.org/10.1175/JAS-D-14-0065.1, 2015.

Morrison, H., Curry, J. A., and Khvorostyanov, V. I.: A New Double-Moment Microphysics Parameterization for Application in Cloud and Climate Models. Part I: Description, Journal of the Atmospheric Sciences, 62, 1665–1677, https://doi.org/10.1175/JAS3446.1, 2005.

Murphy, D. M. and Koop, T.: Review of the Vapour Pressures of Ice and Supercooled Water for Atmospheric Applications, Quarterly Journal of the Royal Meteorological Society, 131, 1539–1565, https://doi.org/10.1256/qj.04.94, 2005.

Ohno, T., Satoh, M., and Noda, A.: Fine Vertical Resolution Radiative-Convective Equilibrium Experiments: Roles of Turbulent Mixing on the High-Cloud Response to Sea Surface Temperatures, Journal of Advances in Modeling Earth Systems, 11, 1–18, https://doi.org/10.1029/2019MS001704, 2019.

Pan, L. L., Atlas, E. L., Salawitch, R. J., Honomichl, S. B., Bresch, J. F., Randel, W. J., Apel, E. C., Hornbrook, R. S., Weinheimer, A. J., Anderson, D. C., Andrews, S. J., Baidar, S., Beaton, S. P., Campos, T. L., Carpenter, L. J., Chen, D., Dix, B., Donets, V., Hall, S. R., Hanisco, T. F., Homeyer, C. R., Huey, L. G., Jensen, J. B., Kaser, L., Kinnison, D. E., Koenig, T. K., Lamarque, J. F., Liu, C., Luo, J., Luo, Z. J., Montzka, D. D., Nicely, J. M., Pierce, R. B., Riemer, D. D., Robinson, T., Romashkin, P., Saiz-Lopez, A., Schauffler, S., Shieh, O., Stell, M. H., Ullmann, K., Vaughan, G., Volkamer, R., and Wolfe, G.: The Convective Transport of Active Species in the Tropics (Contrast) Experiment, Bulletin of the American Meteorological Society, 98, 106–128, https://doi.org/10.1175/BAMS-D-14-00272.1, 2017.

Prein, A. F., Wang, D., Ge, M., Ramos Valle, A., and Chasteen, M. B.: Resolving Mesoscale Convective Systems: Grid Spacing Sensitivity in the Tropics and Midlatitudes, Journal of Geophysical Research: Atmospheres, 130, e2024JD042 530, https://doi.org/10.1029/2024JD042530, 2025.

Proske, U., Ferrachat, S., Klampt, S., Abeling, M., and Lohmann, U.: Addressing Complexity in Global Aerosol Climate Model Cloud Microphysics, Journal of Advances in Modeling Earth Systems, 15, e2022MS003 571, https://doi.org/10.1029/2022MS003571, 2023.

Qu, Z., Korolev, A., Milbrandt, J. A., Heckman, I., Huang, Y., McFarquhar, G. M., Morrison, H., Wolde, M., and Nguyen, C.: The Impacts of Secondary Ice Production on Microphysics and Dynamics in Tropical Convection, Atmospheric Chemistry and Physics, 22, 12 287–12 310, https://doi.org/10.5194/acp-22-12287-2022, 2022.

Salesky, S. T., Gillis, K., Anderson, J., Helman, I., Cantrell, W., and Shaw, R. A.: Modeling the Subgrid-Scale Scalar Variance: A Priori Tests and Application to Supersaturation in Cloud Turbulence, Journal of the Atmospheric Sciences, 81, 839–853, https://doi.org/10.1175/JAS-D-23-0163.1, 2024.

Scott, S. G., Bui, T. P., Chan, K. R., and Bowen, S. W.: The Meteorological Measurement System on the NASA ER-2 Aircraft, Journal of Atmospheric and Oceanic Technology, 7, 525–540, https://doi.org/10.1175/1520-0426(1990)007<0525:TMMSOT>2.0.CO;2, 1990.

Seiki, T. and Ohno, T.: Improvements of the Double-Moment Bulk Cloud Microphysics Scheme in the Nonhydrostatic Icosahedral Atmospheric Model (NICAM), Journal of the Atmospheric Sciences, 80, 111–127, https://doi.org/10.1175/JAS-D-22-0049.1, 2022.

Shardt, N., N. Isenrich, F., Waser, B., Marcolli, C., A. Kanji, Z., J. deMello, A., and Lohmann, U.: Homogeneous Freezing of Water Droplets for Different Volumes and Cooling Rates, Physical Chemistry Chemical Physics, 24, 28 213–28 221, https://doi.org/10.1039/D2CP03896J, 2022.

Sherwood, S. C., Webb, M. J., Annan, J. D., Armour, K. C., Forster, P. M., Hargreaves, J. C., Hegerl, G., Klein, S. A., Marvel, K. D., Rohling, E. J., Watanabe, M., Andrews, T., Braconnot, P., Bretherton, C. S., Foster, G. L., Hausfather, Z., Heydt, A. S., Knutti, R., Mauritsen, T., Norris, J. R., Proistosescu, C., Rugenstein, M., Schmidt, G. A., Tokarska, K. B., and Zelinka, M. D.: An Assessment of Earth's Climate Sensitivity Using Multiple Lines of Evidence, Reviews of Geophysics, 58, 1–92, https://doi.org/10.1029/2019rg000678, 2020.

Shi, X., Liu, X., and Zhang, K.: Effects of Preexisting Ice Crystals on Cirrus Clouds and Comparison between Different Ice Nucleation Parameterizations with the Community Atmosphere Model (CAM5), Atmospheric Chemistry and Physics, 15, 1503–1520, https://doi.org/10.5194/acp-15-1503-2015, 2015.

Silvers, L. G., Reed, K. A., and Wing, A. A.: The Response of the Large-Scale Tropical Circulation to Warming, Journal of Advances in Modeling Earth Systems, 15, e2021MS002 966, https://doi.org/10.1029/2021MS002966, 2023.

Sokol, A. B. and Hartmann, D. L.: Tropical Anvil Clouds: Radiative Driving Toward a Preferred State, Journal of Geophysical Research: Atmospheres, 125, e2020JD033 107, https://doi.org/10.1029/2020JD033107, 2020.

Sokol, A. B., Wall, C. J., and Hartmann, D. L.: Greater Climate Sensitivity Implied by Anvil Cloud Thinning, Nature Geoscience, pp. 1–6, https://doi.org/10.1038/s41561-024-01420-6, 2024.

Sourdeval, O., C.-Labonnote, L., Baran, A. J., Mülmenstädt, J., and Brogniez, G.: A Methodology for Simultaneous Retrieval of Ice and Liquid Water Cloud Properties. Part 2: Near-global Retrievals and Evaluation against A-Train Products, Quarterly Journal of the Royal Meteorological Society, 142, 3063–3081, https://doi.org/10.1002/qj.2889, 2016.

Stephens, G. L., Vane, D. G., Tanelli, S., Im, E., Durden, S., Rokey, M., Reinke, D., Partain, P., Mace, G. G., Austin, R., L'Ecuyer, T. S., Haynes, J., Lebsock, M., Suzuki, K., Waliser, D., Wu, D., Kay, J., Gettelman, A., Wang, Z., and Marchand, R.: CloudSat Mission: Performance and Early Science after the First Year of Operation, Journal of Geophysical Research Atmospheres, 114, 1–18, https://doi.org/10.1029/2008JD009982, 2008.

Stevens, B., Satoh, M., Auger, L., Biercamp, J., Bretherton, C. S., Chen, X., Düben, P., Judt, F., Khairoutdinov, M., Klocke, D., Kodama, C., Kornblueh, L., Lin, S. J., Neumann, P., Putman, W. M., Röber, N., Shibuya, R., Vanniere, B., Vidale, P. L., Wedi, N., and Zhou, L.: DYAMOND: The DYnamics of the Atmospheric General Circulation Modeled On Non-hydrostatic Domains, Progress in Earth and Planetary Science, 6, https://doi.org/10.1186/s40645-019-0304-z, 2019.

Sullivan, S., Voigt, A., Miltenberger, A., Rolf, C., and Krämer, M.: A Lagrangian Perspective of Microphysical Impact on Ice Cloud Evolution and Radiative Heating, Journal of Advances in Modeling Earth Systems, 14, e2022MS003 226, https://doi.org/10.1029/2022MS003226, 2022.

Thompson, G., Field, P. R., Rasmussen, R. M., and Hall, W. D.: Explicit Forecasts of Winter Precipitation Using an Improved Bulk Microphysics Scheme. Part II: Implementation of a New Snow Parameterization, Monthly Weather Review, 136, 5095–5115, https://doi.org/10.1175/2008MWR2387.1, 2008.

Turbeville, S. M., Nugent, J. M., Ackerman, T. P., Bretherton, C. S., and Blossey, P. N.: Tropical Cirrus in Global Storm-Resolving Models: 2. Cirrus Life Cycle and Top-of-Atmosphere Radiative Fluxes, Earth and Space Science, 9, e2021EA001 978, https://doi.org/10.1029/2021EA001978, 2022.

Voigt, A., Albern, N., and Papavasileiou, G.: The Atmospheric Pathway of the Cloud-Radiative Impact on the Circulation Response to Global Warming: Important and Uncertain, Journal of Climate, 32, 3051–3067, https://doi.org/10.1175/JCLI-D-18-0810.1, 2019.

Voigt, A., North, S., Gasparini, B., and Ham, S.-H.: Atmospheric Cloud-Radiative Heating in CMIP6 and Observations and Its Response to Surface Warming, Atmospheric Chemistry and Physics, 24, 9749–9775, https://doi.org/10.5194/acp-24-9749-2024, 2024.

Wall, C. J. and Hartmann, D. L.: Balanced Cloud Radiative Effects Across a Range of Dynamical Conditions Over the Tropical West Pacific, Geophysical Research Letters, 5, 490–498, https://doi.org/10.1029/2018GL080046, 2018.

Wall, C. J., Norris, J. R., Gasparini, B., Smith, W. L., Thieman, M. M., and Sourdeval, O.: Observational Evidence That Radiative Heating Modifies the Life Cycle of Tropical Anvil Clouds, Journal of Climate, 33, 8621–8640, https://doi.org/10.1175/JCLI-D-20-0204.1, 2020.

Wernli, H., Boettcher, M., Joos, H., Miltenberger, A. K., and Spichtinger, P.: A Trajectory-Based Classification of ERA-Interim Ice Clouds in the Region of the North Atlantic Storm Track, Geophysical Research Letters, 43, 1–8, https://doi.org/10.1002/2016GL068922., 2016.

Wielicki, B. A., Barkstrom, B. R., Harrison, E. F., Lee, R. B., Smith, G. L., and Cooper, J. E.: Clouds and the Earth's Radiant Energy System (CERES): An Earth Observing System Experiment, Bulletin of the American Meteorological Society, 77, 853–868, https://doi.org/10.1175/1520-0477(1996)077<0853:CATERE>2.0.CO;2, 1996.

Wing, A. A., Reed, K. A., Satoh, M., Stevens, B., Ohno, T., and Bony, S.: Radiative–Convective Equilibrium Model Intercomparison Project, Geoscientific Model Development, 11, 793–813, https://doi.org/10.5194/gmd-11-793-2018, 2018.

Wing, A. A., Silvers, L. G., and Reed, K. A.: RCEMIP-II: Mock-Walker Simulations as Phase II of the Radiative-Convective Equilibrium Model Intercomparison Project, Preprint, Atmospheric sciences, https://doi.org/10.5194/gmd-2023-235, 2023.

Winker, D. M., Pelon, J., Coakley, J. A., Ackerman, S. A., Charlson, R. J., Colarco, P. R., Flamant, P., Fu, Q., Hoff, R. M., Kittaka, C., Kubar, T. L., Le Treut, H., McCormick, M. P., Mégie, G., Poole, L., Powell, K., Trepte, K., Vaughan, M. A., and Wielicki, B. A.: The Calipso Mission: A Global 3D View of Aerosols and Clouds, Bulletin of the American Meteorological Society, 91, 1211–1229, https://doi.org/10.1175/2010BAMS3009.1, 2010.

Yang, Q., Fu, Q., Austin, J., Gettelman, A., Li, F., and Vömel, H.: Observationally Derived and General Circulation Model Simulated Tropical Stratospheric Upward Mass Fluxes, Journal of Geophysical Research: Atmospheres, 113, https://doi.org/10.1029/2008JD009945, 2008.